Clim Dyn (2018) 50:3457–3484
DOI 10.1007/s00382-017-3817-4

# Differences in mass balance behavior for three glaciers from different climatic regions on the Tibetan Plateau

**Meilin Zhu[1] · Tandong Yao[1,2] · Wei Yang[1,2] · Baiqing Xu[1,2] · Guanjian Wu[1,2] · Xiaojun Wang[3]**

Received: 17 January 2017 / Accepted: 16 July 2017 / Published online: 21 July 2017


**Abstract** Glacier mass balance shows a spatially heterogeneous pattern in response to global warming on the Tibetan Plateau (TP), and the climate mechanisms controlling this pattern require further study. In this study, three glaciers where systematic glaciological and meteorological observations have been carried out were selected, specifically Parlung No. 4 (PL04) and Zhadang (ZD) glaciers on the southern TP and Muztag Ata No. 15 (MZ15) glacier in the eastern Pamir. The characteristics of the mass and energy balances of these three glaciers during the periods between October 1th, 2008 and September 23rd, 2013 were analyzed and compared using the energy and mass balance model. Results show that differences in surface melt, which mainly result from differences in the amounts of incoming longwave radiation ($L_{in}$) and outgoing shortwave radiation ($S_{out}$), represent the largest source of the observed differences in mass balance changes between PL04 and ZD glaciers and MZ15 glacier, where air temperature, humidity, precipitation and cloudiness are dramatically different. In addition, sensitivity experiments show that mass balance sensitivity to air temperature change is remarkably higher than that associated with precipitation change on PL04 and ZD glaciers, in contrast results from MZ15 glacier. And significantly higher sensitivities to air temperature change are noted for PL04 and ZD glaciers than for MZ15 glacier. These significant differences in the sensitivities to air temperature change are mainly caused by differences in the ratio of snowfall to precipitation during the ablation season, melt energy ($L_{in}$+$S_{out}$) during the ablation season and the seasonality of precipitation among the different regions occupied by glaciers. In turn, these conditions are related to local climatic conditions, especially air temperature. These factors can be used to explain the different patterns of change in Tibetan glacier mass balance under global warming.

**Keyword** Glacier mass and energy balance · Global warming · Climate characteristics · Climate sensitivity · Tibetan Plateau

## 1 Introduction

The Tibetan Plateau (TP) and the surrounding mountains contain most of the glaciers situated within the middle and low latitude regions. These glaciers cover a total area of approximately 100,000 km$^2$ (Pfeffer et al. 2014; Yao et al. 2012). These glaciers play a crucial role in supplying water to Asia's main river basins (Immerzeel et al. 2010) and can cause glacier lake outburst floods (Wang et al. 2011). In the past few decades, air temperature ($T_a$) over the TP has increased, as has been proven by several studies using meteorological measurements (Liu and Chen 2000; Zhang et al. 2015) and ice core records (Yao et al. 2000). Against this background, most of the Tibetan glaciers rapidly

**Electronic supplementary material** The online version of this article (doi:10.1007/s00382-017-3817-4) contains supplementary material, which is available to authorized users.

✉ Meilin Zhu
meilinzhu@itpcas.ac.cn

[1] Key Laboratory of Tibetan Environment Changes and Land Surface Processes, Institute of Tibetan Plateau Research, Chinese Academy of Sciences (CAS), Building 3, Courtyard 16, Lincui Road, Chaoyang District, Beijing 100101, China

[2] CAS Center for Excellence in Tibetan Plateau Earth Sciences, Beijing 100101, China

[3] Institute of Agricultural Economics and Development, Chinese Academy of Agricultural Sciences, No.12, Zhongguancun South Road, Haidian, Beijing 100081, China

retreated and lost much of their mass (Bolch et al. 2012, Pu et al. 2008; Wagnon et al. 2013; Wang et al. 2010; Yao et al. 2012). However, some of the glaciers within the region—the Western Kunlun mountains, eastern Pamir and Karakoram mountains—have shown slight mass gains or balanced mass budgets during the period 2000–2010, which was determined using remote sensing observations of regional glacier covered areas or direct mass balance records of several typical glaciers (Bolch et al. 2012; Gardelle et al. 2013; Gardner et al. 2013; Hewitt 2005; Kääb et al. 2015; Neckel et al. 2014).

The climatic mechanisms controlling the spatially heterogeneous changes in Tibetan glaciers described above remain unclear, and there is substantial debate on this point. The main debate is whether $T_a$ or precipitation ($P$) is more important in controlling the differences in mass balance changes seen on the TP. Some studies have argued that the relative stability of glaciers in the Pamir and Karakoram can be attributed to increases in $P$ from the strengthened westerlies (Bolch et al. 2012; Gardelle et al. 2013; Yao et al. 2012). Kapnick et al. (2014) found that the non-monsoonal winter $P$ led to the Karakoram Anomaly. The above studies all stressed that $P$ played the most important role in producing the Karakoram Anomaly. Nevertheless, Zafar et al. (2016) thought that the region's $T_a$ and cloudiness contributed to the Karakoram Anomaly. Similarly, debate about the climatic mechanisms controlling glacier changes in the monsoon region of the TP also exists (Fujita and Nuimura 2011; Salerno et al. 2015; Xu et al. 2009; Yang et al. 2016). In addition, a few studies have suggested that atmospheric circulation patterns and terrain factors (e.g. aspect, size, shape, altitudinal range, and especially hypsography) were also important factors in determining glacier mass balance changes on and around the TP (Liu and Liu 2015; Mölg et al. 2014; Oerlemans et al. 1998; Yang et al. 2011). However, atmospheric circulation patterns and terrain factors influence glacier mass balance by changing local $T_a$ and $P$. Thus, the factors that directly influence glacier mass balance are $T_a$ and $P$.

An understanding of the direct influence of $T_a$ and $P$ on glacier mass balance requires an abundance of glacio-meteorological measurement data to quantitatively assess surface energy balances and their relation to glacier mass balances. However, few glaciers on the TP have been continuously observed for glacier mass balance and glacio-meteorology (Fujita and Ageta 2000; Sun et al. 2014; Wu et al. 2016; Yang et al. 2011; Zhang et al. 2013). In addition, the studies were based on these observed glaciers and mainly discussed the climatic mechanisms that control the variations in single glaciers or several glaciers within the same climatic region, either within the South Asian monsoon (SAM) region (Fujita and Nuimura 2011; Huintjes et al. 2015; Mölg et al. 2014; Yang et al. 2015; Zhang et al. 2012) or in the westerly region (Sun et al. 2012; Wu et al. 2016). Studies that only focus on single glaciers or several glaciers under the same climatic region cannot provide a clear explanation of glacier change over the TP as a whole, because the TP contains a variety of climate settings (Maussion et al. 2013; Mölg et al. 2014; Rupper et al. 2009). Moreover, comparative analyses of glacier-wide energy and mass balance processes and climate sensitivity among glaciers within different climatic regions on the TP based on measured glacio-meteorological data have not been carried out in previous studies. Only Huintjes (2014) compared the energy and mass balance components of five glaciers in different regions on the TP based on meteorological data from the Weather Research & Forecasting Model (WRF). Such comparisons require some level of meteorological, glaciological or remote sensing-based field observations to limit constrain their modelling. This requirement brings about limitations in providing improved explanations of the relationships between climate factors and glacier variations. To obtain reliable and detailed glacier energy and mass balance estimates based on complex modelling, basic in-situ measurements at glaciers on the TP are a crucial requirement (Huintjes 2014).

To explore the fundamental mechanisms responsible for the differences in mass balance changes on the TP in different climatic regions under global warming, three glaciers were selected, the Parlung No. 4 (PL04) and Zhadang (ZD) glaciers on the southern TP and the Muztag Ata No. 15 (MZ15) glacier in the eastern Pamir, where systematic glaciological and meteorological observations have been carried out. Differences in the glacier-wide meteorological characteristics, as well as their mass and energy balances, were analyzed using the energy and mass balance (EMB) model. In addition, the factors that produced the different sensitivities of the mass balances of the three glaciers to $T_a$ change and $P$ change were used to analyze the differences in spatial pattern of glacier mass balance changes in different regions on the TP under global warming. The research results have practical implications for understanding the spatially heterogeneity of glacier mass balance changes, improving our ability to simulate glacier discharges, guiding the use of water resources in the arid zones downstream and improving our ability to predict glacier hazards on the TP.

## 2 Study area and field measurement

### 2.1 Study area and AWS sites

PL04 glacier (29°14′N, 96°55′E) is a typical valley-type glacier that lies in the Parlung-Zangbu River Basin on the southeast TP. It is affected by the SAM in summer and

by the westerlies in winter (Fig. 1). The glacier is debris free and flows northward from an elevation of 5937 m to 4657 m, with a length of nearly 8 km (Shi et al. 2008) and an area of approximately 11.86 km$^2$, according to the Second Chinese Glacier Inventory (Guo et al. 2015). Its equilibrium line altitude (ELA) was 5452 m in 2005–2006, whereas its mass balance was −0.73 m w.e. (Yao et al. 2010). The annual rate of terminal retreat in recent years has been approximately 15 m/year (Yang et al. 2010). According to the Zayu national meteorological station (97°28′E, 28°39′N, 2327.6 m), which lies approximately 90 km from PL04 glacier, *P* occurs mainly from spring to summer. Three AWSs (AWS1-P, AWS2-P and AWS3-P) were deployed near or on PL04 glacier. AWS1-P is located 5 km north of the glacier snout and was installed on a lateral moraine at 4600 m a.s.l. in June 2006. AWS2-P (4800 m a.s.l.) and AWS3-P (5202 m a.s.l.) have been in operation on PL04 glacier since May 2009 and from July 2010 to August 2012, respectively. Detailed information about the three AWSs can be found in Yang et al. (2011, 2013) and Zhu et al. (2015).

ZD glacier (30°29′N, 90°39′E) is located on the northern slope of the western Nyainqentanglha Range on the southern TP and is affected by the SAM in summer and the westerlies in winter (Fig. 1). It is a typical valley-type glacier without debris cover. This glacier faces north-northwest and ranges in altitude from 5515 m to 5947 m. Its length is about 2.2 km (Zhang et al. 2013), and its area is approximately 1.8 km$^2$. The ELA of this glacier lay at approximately 5840, 5870 and 5640 m a.s.l., and its mass balance was −1.1, −0.8 and −0.2 m w.e. during 2005–2006, 2006–2007 and 2007–2008 (Yu et al. 2013). Huintjes et al. (2015) reported that the modelled annual mean glacier-wide mass balance of ZD glacier was $-1.067 \pm 0.6$ m w.e. in 2001–2011. And Mölg et al. (2014) reported that it was $-0.891 \pm 0.105$ m w.e. for the same period. The annual rate of terminal retreat in recent years (2001–2012) was approximately 10.6 m/year (Bolch et al. 2010). According to the Damxung national meteorological station (91°06′E,

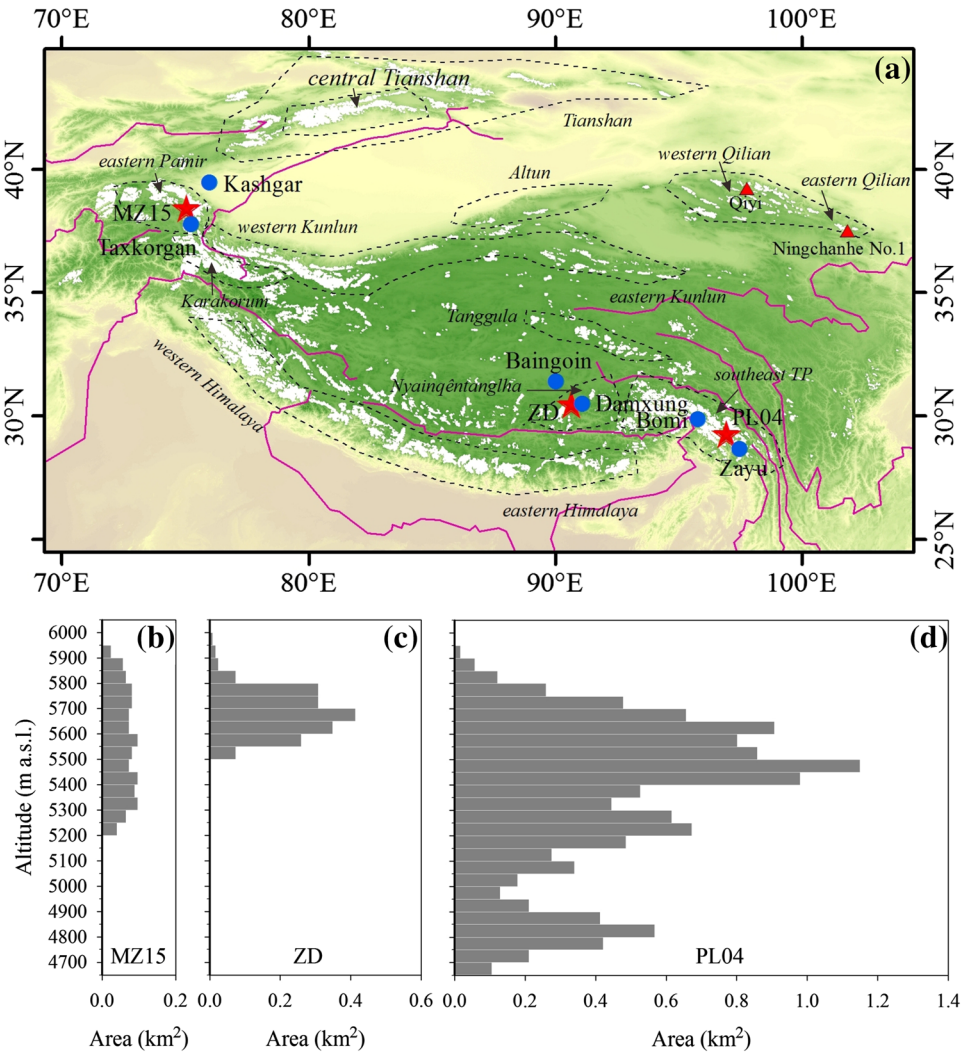


**Fig. 1** Locations of three studied glaciers (*red star*), six Chinese meteorological stations (*blue point*) near the glaciers, and two other glaciers (*red triangles*) on the Tibetan Plateau, as well as name of mountain ranges (*italics* and *dashed outline*) (**a**); the site of Muztag Ata No. 15 (MZ15) glacier (*black outline*) and distribution of the four AWSs (*green point*) in the Muztag Ata region (**b**). Satellite image taken by Landsat TM in September 2008 and area-altitude distribution of Muztag Ata No. 15 (MZ15) glacier (**c**), Zhadang (ZD) glacier (**d**) and Parlung No. 4 (PL04) glacier (**e**)

30°29′N, 4200 m), which lies roughly 44 km from ZD glacier, $P$ is concentrated in summer. Two almost identical AWSs (named AWS1-Z and AWS2-Z) were installed in the middle section of this glacier (at 5665 m a.s.l.) in May 2009 and near the terminus (5566 m a.s.l.) in October 2010, respectively. Detailed information on the two AWSs can be found in Mölg et al. (2012).

MZ15 glacier (38°14´N, 75°03´E) is located in the eastern Pamir and is affected by the westerlies throughout the year (Yao et al. 2012) (Fig. 1 and S1). This glacier is debris free, with an area of approximately 1.09 km$^2$ (Guo et al. 2015), and a length of 1.8 km (Yao et al. 2012). Its altitudinal range is between 5237 m and 5935 m. This glacier faces west. Its mean ELA was 5640 m a.s.l., and its annual mean mass balance was 0.248 m w.e. during 2005–2010 (Yao et al. 2012). The annual rate of terminal retreat in recent years (2001–2012) was approximately 1.7 m/year (Yao et al. 2012). Precipitation is concentrated from April to September, according to data from the Taxkorgen national meteorological station. Four AWSs (AWS1-M, AWS2-M, AWS3-M and AWS4-M) were deployed near MZ15 glacier (Fig. 1) to obtain basic meteorological data for the EMB model. AWS1-M (3655 m a.s.l.), located on sandy ground, was installed in October 2009. AWS2-M, located 5.2 km north of MZ15 glacier, was installed on a lateral moraine of Kartamak glacier at 4400 m a.s.l. in July 2009. AWS3-M (4900 m a.s.l.), located on one of the slopes of Muztag Ata Peak, was installed in August 2011. In addition, AWS4-M (5900 m a.s.l.) was operated on a glacier on Muztag Ata Peak from September 2011 to July 2012.

### 2.2 Mass balance data

Measurements of glacier mass balance were made using glaciological methods (Paterson 1994). Only two sites with measured mass balance data were available on PL04 glacier. One site was near AWS2-P and measurements of stake mass balance were made there from May 2009 to September 2009 (Yang et al. 2011). The other site was at AWS3-P, which recorded surface heights using the Campbell SR50 sonic ranging sensor. In addition, stake mass balance of Parlung No. 94 (PL94) glacier was obtained from Yang et al. (2013) and WGMS (2015) and was used to validate the simulation results of PL04 glacier.

Several stakes on ZD glacier were used to evaluate the model results. The locations of these stakes were presented in Huintjes et al. (2015). Stake readings were available for three intervals: the first one in June–July 2009, the second one in September 2009–May 2010 and the third one in August–September 2010. In addition, five-year glacier-wide mass balance measurements were made from 2008 to 2013 on ZD glacier.

For MZ15 glacier, monitoring stakes were distributed over the glacier surface from September 2008 to September 2013, except in 2009. The height of each stake was measured in September every year. When snow cover appeared near these stakes, snow pits were dug to measure snow layer density and stratigraphy. The mass balance and snowpack height data were used to validate the performance of the EMB model.

### 2.3 Meteorological measurements

The data from AWS2-P, AWS1-Z and AWS2-M, which were initially set up in May 2009 on PL04 glacier, in May 2009 on ZD glacier and in September 2009 near MZ15 glacier, respectively, were used to drive the EMB model. From these AWSs, incoming shortwave radiation ($S_{in}$), outgoing shortwave radiation ($S_{out}$), net radiation ($R_{net}$), incoming longwave radiation ($L_{in}$), surface temperature ($T_S$) (or outgoing longwave radiation ($L_{out}$)), $T_a$, relative humidity ($RH$), air pressure ($P_a$), wind speed ($WS$) and wind direction ($WD$) can be obtained. It is noteworthy that $L_{in}$ is not directly measured at AWS1-Z. Instead, it is calculated as a residual from measured $R_{net}$, $L_{out}$ (obtained from the measured $T_S$ by the Stefan–Boltzmann law), $S_{in}$ and $S_{out}$ (Table 1). $P$ was obtained from three all-weather precipitation gauges (T-200B) equipped with hanging weighing transducers that were installed close to PL04 glacier at an altitude of 4600 m a.s.l., near ZD glacier at an altitude of 5580 m a.s.l. and near MZ15 glacier at an altitude of 3655 m a.s.l., respectively. The SR50 sonic ranging sensors were deployed at AWS1-Z and AWS3-P to measure glacier surface heights. $S_{in}$ recorded at AWS1-M and AWS4-M and $L_{in}$ recorded at AWS1-M and AWS2-M were used to check the performance of parameterizations of $S_{in}$ and $L_{in}$ at different altitudes. Detailed specifications of these AWSs can be found in Table 1 and the recently published studies of Yang et al. (2011), Mölg et al. (2012) and Zhu et al. (2015).

Data from the China Meteorological Forcing Dataset (CMFD), which has a resolution of 0.1° × 0.1° (He and Yang 2011), Chinese national meteorological stations (CMS), and the High Asia Refined analysis with a resolution of 10 km (HAR10) which is generated using the atmospheric model WRF version 3.3.1 (Maussion et al. 2013), were used to produce a continuous meteorological dataset for each of the three glaciers from 2008 to 2013. Moreover, monthly $S_{out}$, $L_{in}$, snowfall and $P$ from the HAR with a resolution of 30 km (HAR30) are used to analyze the spatial distribution of Tibetan glacier mass balance changes.

**Table 1** Sensors information and technical specifications of the AWSs

| Parameters | Sensors | Accuracy | Location |
|---|---|---|---|
| $T_a$ | Vaisala HMP 45 C | ±0.2 °C (−40 to +60 °C) | AWS2-M, AWS2-P |
| | Campbell CS215 | ±0.9 °C (−40 to +70 °C) | AWS1-Z |
| *RH* | Vaisala HMP 45 C | ±2% (0–100%) | AWS2-M, AWS2-P |
| | Campbell CS215 | ±4% (0–100%) | AWS1-Z |
| *WS* | Young 05103 wind monitor | ±0.3 m/s | AWS2-M, AWS2-P, AWS1-Z |
| *P* | T-200B | ±0.6 mm | AWS1-P, AWS1-Z, AWS1-M |
| $S_{in}/S_{out}$ | Kipp and Zonen CNR1 | ±10% | AWS1-M, AWS2-M, AWS4-M, AWS2-P |
| | Campbell CS300 | 5% for daily totals | AWS3-P, AWS1-Z |
| $L_{in}/L_{out}$ | Kipp and Zonen CNR1 | ±10% | AWS1-M, AWS2-M, AWS3-M, AWS2-P |
| $R_{net}$ | Campbell NR-LITE | 20% (assumption) | AWS1-Z |
| $T_S$ | Campbell IRTS-P | 0.3 °C | AWS1-Z |
| Surface height | Campbell SR50 | 1 cm | AWS3-P, AWS1-Z |

$T_a$ air temperature (°C), *RH* relative humidity (%), *WS* wind speed (m/s), *P* precipitation (mm), $S_{in}$ and $S_{out}$ incoming and outgoing shortwave radiation (W/m$^2$), $L_{in}$ and $L_{out}$ incoming and outgoing longwave radiation (W/m$^2$), $R_{net}$ net radiation (W/m$^2$), $T_S$ surface temperature (°C), $L_{in}$ at AWS1-Z is a residual calculated from the measured values of $S_{in}$, $S_{out}$, $R_{net}$ and $T_S$

## 3 Methods

### 3.1 Data processing

The meteorological data were recorded by the AWSs for the three glaciers from 2009 to 2013. However, due to harsh environmental conditions that occur at high elevations, a significant amount of meteorological data was lost, and this missing data needed to be filled in. To produce a continuous meteorological dataset for the three glaciers from 2008 to 2013, data from the CMS and the grid points that contain the sites of the AWS measurements used to drive the model of the CMFD and the HAR10 were downscaled to the site of each AWS using its measurements (the driving data). In addition, the data from AWS1-P near PL04 glacier were also downscaled to the site of AWS2-P using data measured from AWS2-P. The downscaling method is the same as that used by Yang et al. (2016).

$S_{in}$ values from the CMFD with a 3-hourly resolution were downscaled to a resolution of 1 h by interpolation. Monthly coefficients for hourly $S_{in}$, daily mean $T_a$, daily mean *RH* and daily mean *WS* were calculated by linear regression analysis each month (Yang et al. 2015). Based on the monthly coefficients, multi-reconstructed data could be obtained. In addition, these reconstructions were compared with the measurement data. Finally, for each glacier, the best reconstructed data were selected. For PL04 glacier, $T_a$ and *RH* from AWS1-P and *WS* from HAR10 were corrected using their respective monthly coefficients. $S_{in}$ values from the AWS1-P dataset were used directly in the model because of their good agreement with the in situ measurements recorded by AWS2-P. For ZD and MZ15 glaciers, $T_a$, *RH* and *WS* values from the HAR10 were corrected using their corresponding monthly coefficients. $S_{in}$ values from the CMFD were corrected using the relevant monthly coefficients. The values of the root mean square error (RMSE) and correlation coefficient (R) between these measured meteorological variables and the reconstructed data are shown in Table 2.

To fill the gaps in measurements of *P* recorded by the T-200B units on the three glaciers, *P* values from the CMFD, the HAR10 and the CMS were corrected using the method of Yang et al. (2013). It is found that *P* values from the CMFD, the HAR10 and Taxkorgen national

**Table 2** Origin data used for reconstructing input meteorological variables and the performance of reconstructed input meteorological variables at each AWS

| | PL04 | | | ZD | | | MZ15 | | |
|---|---|---|---|---|---|---|---|---|---|
| | Origin | RMSE | R | Origin | RMSE | R | Origin | RMSE | R |
| *P* (mm) | ITP | – | – | HAR10 | – | – | TX | – | – |
| $T_a$ (℃) | AWS1-P | 1.6 | 0.97 | HAR10 | 1.4 | 0.98 | HAR10 | 1.7 | 0.97 |
| *RH* (%) | AWS1-P | 8.8 | 0.82 | HAR10 | 11.8 | 0.84 | HAR10 | 13.8 | 0.69 |
| *WS* (m/s) | HAR10 | 1.2 | 0.59 | HAR10 | 1.1 | 0.62 | HAR10 | 1.8 | 0.78 |
| $S_{in}$ (W/m$^2$) | AWS2-P | 1.6 | 0.97 | ITP | 32.1 | 0.87 | ITP | 37.7 | 0.91 |

R denotes the correlation coefficient (while $p < 0.005$); RMSE is the root mean square error

meteorological station agree well with the measurements for PL04, ZD and MZ15 glaciers, respectively, by comparing $P$ from a cumulative number of events, as well as the cumulative amount and seasonal distribution between the measured and corrected data (Fig. S2).

### 3.2 The energy and mass balance model

The EMB model used in this study is based on the point energy and mass balance model presented by Zhu et al. (2015). Here we mainly present the most important features of the model. The model solves the following equation:

$$M = \int \left( \frac{Q_M}{L_m} + \frac{H_{lat}}{L_v} + C_{en} + P_{snow} \right) dt \quad (1)$$

where point mass balance ($M$) is composed of melting ($\frac{Q_M}{L_m}$), sublimation/evaporation ($\frac{H_{lat}}{L_v}$), refreezing ($C_{en}$) and solid precipitation ($P_{snow}$). $L_m$ is the latent heat of ice melt and $L_v$ is the latent heat of evaporation/sublimation. Melt energy ($Q_M$) is calculated using the surface energy balance equation:

$$Q_M = S_{in}(1-\alpha) + L_{in} + L_{out} + H_{sen} + H_{lat} + QG \quad (2)$$

where $\alpha$ is the albedo. $H_{sen}$ and $H_{lat}$ are the sensible and latent heat fluxes and $QG$ is the subsurface heat flux. $QG$ consists of a conductive heat flux ($G$) and an energy flux due to penetrating shortwave radiation ($QPS$). Net shortwave and longwave radiation is written as $S_{net}$ and $L_{net}$, respectively. $R_{net}$ is the sum of $S_{net}$ and $L_{net}$. All fluxes are defined as positive when they are directed towards the surface.

Based on the latest model version (Yang et al. 2013; Zhu et al. 2015), we added a few new features with reference to several published works. The equations of these new features are presented in Supplementary Appendix B for the sake of simplicity. First, $S_{in}$ consists of direct solar radiation, diffuse solar radiation and reflected solar radiation from the ground. Direct solar radiation, diffuse solar radiation and reflected solar radiation from the ground are calculated according to Brock and Arnold (2000). Topographic shading has an effect on the receipt of direct solar radiation (Arnold et al. 1996), and it is calculated on the hourly scale using the method proposed by Hock and Holmgren (2005). The $S_{in}$ received at each glacier grid point is the sum of the total diffuse radiation, the correct proportion of the direct radiation corresponding to the unshaded area, and the reflected solar radiation from the ground. To check the ability of the parameterization to reproduce the correct $S_{in}$ values at different altitudes, we tested this parameterization at three AWSs in the Muztag Ata region. The RMSE values reflecting the differences between the modelled and observed daily mean $S_{in}$ values were 28, 21 and 38 W/m$^2$, and the corresponding R values were 0.95, 0.99 and 0.94, at AWS1-M, AWS2-M and AWS4-M, respectively (Fig. S6). Second, the surface $L_{in}$ is modelled by the method of Sicart et al. (2011), which accounts for longwave emissions from the surrounding slopes and sky. Transmissivity ($\tau$) is calculated as the ratio of measured $S_{in}$ and clear-sky solar radiation at the top of the atmosphere (Sicart et al. 2011; Zhu et al. 2017). To test the performance of the $L_{in}$ model at different altitudes within the same region, the parameterization was checked at the AWSs in the Muztag Ata region. The parameters of the $L_{in}$ model were optimized at AWS2-M on MZ15 glacier. According to the optimized parameters, $T_a$, $RH$, $\tau$ and $S_{in}$ from AWS2-M, the air temperature lapse rate ($T_{rate}$) and the terrain factors at AWS1-M and AWS3-M and $L_{in}$ at AWS1-M and AWS3-M were modelled. The RMSE values reflecting the differences between the modelled and observed daily mean $L_{in}$ values were 16.1 W/m$^2$, 15.5 W/m$^2$ and 17.8 W/m$^2$, and the corresponding R values were 0.95, 0.94 and 0.92, at AWS1-M, AWS2-M and AWS3-M, respectively (Fig. S7). The detailed parameters of the model are presented in Table S3.

### 3.3 Initial conditions

The EMB model ran on the SRTM digital elevation model, which has a grid spacing of 90 m, for the three glaciers. The shapes of PL04 and MZ15 glaciers were obtained from the Second Glacier Inventory Dataset of China (Version 1.0) (Guo et al. 2014). The outline of ZD glacier was determined from Landsat TM 2008 image, and this outline is identical to that used by Huintjes et al. (2015) and Yu et al. (2013). When the model began running, August 15th, 2008, the initial snow depth was set to 0 m at all grids on PL04 glacier, as there was no snow cover on PL94 glacier (Yang et al. 2013). In addition, for August 15th, 2008, it was set to increase linearly with altitude on ZD glacier, according to snow depth measurements made at the stakes in 2009. This initialization procedure had no influence on the performance of the EMB model shown in Figs. 5 and 6. For September 3rd, 2008, the initial snow depth on MZ15 glacier was set to increase linearly along with altitude, based on measurements made at snow pits at different altitudes. The initial snow densities were set to 410 kg/m$^3$ on ZD and MZ15 glaciers, according to snow pit measurements made on MZ15 glacier. The initial and boundary conditions of the EMB model are shown in Table 3.

Figures S3–S5 shows the sets of observed daily data (Ta, RH, WS, P and Sin) that were used to run the EMB model for the three glaciers. The values of WS and RH measured at the AWSs are assumed to be representative for all of the calculated grid points. The undercatch of measured P that is shown in Table 3 was calculated by the methods of Ma et al. (2015). Then, P values from

**Table 3** Input parameters for the energy and mass balance model on PL04, ZD and MZ15 glaciers

| Abbreviation | Parameter | Values | | |
|---|---|---|---|---|
| | | PL04 | ZD | MZ15 |
| $T_{rate}$ (ºC/100 m) | Vertical air temperature gradient | −0.38[a] | **−0.7** | **−0.67** |
| $P_{rate}$ (%/m) | Vertical precipitation gradient | **0.25** | **0.046** | **0.055** |
| $P_{corr}$ (%) | Precipitation correction | 30[b] | 17[b] | 37[b] |
| $Pres_{srate}$ (hpa/100 m) | Vertical air pressure gradient | **−7.1** | −6.7[c] | **−7.58** |
| $Z_{th}$ (cm) | Snowfall event threshold | 3.8[d] | 5[e] | 8[a] |
| $T_{snow}$ (°C) | Phase threshold for snow | −0.5[d] | 1[f] | 0[g] |
| $T_{rain}$ (°C) | Phase threshold for rain | 1.8[d] | 6.5 [f] | 2[g] |
| *PP_snow* | Fraction of $S_{net}$ absorbed in snow surface layer | 0.05[a] | 0.05[a] | 0.02[a] |
| *PP_ice* | Fraction of $S_{net}$ absorbed in ice surface layer | 0.11[a] | 0.08[a] | 0.04[a] |
| $\alpha_{snow}$ | Fresh snow albedo | **0.83** | **0.8** | 0.83[a] |
| $\alpha_{firn}$ | Firn albedo | **0.5** | **0.58** | 0.53[a] |
| $t^*$ (day) | Albedo time scale | **3.11** | **6** | 6[a] |
| $d^*$ (cm) | Albedo depth scale | **5.743** | **8** | 8[a] |
| $a$ ($°C^{-1}$) | Parameter of ice albedo | **−0.0313** | **−0.0438** | −0.0158[a] |
| $b$ | Parameter of ice albedo | **0.2577** | **0.2157** | 0.1577[a] |
| $C1$ ((K/hPa)$^{C2}$) | Parameter of $L_{in}$ | **1.1405** | **1.1468** | **1.034** |
| $C2$ | Parameter of $L_{in}$ | **7.2809** | **8.899** | **8.634** |
| $C3$ | Parameter of $L_{in}$ | **1.6129** | **1.269** | **1.644** |
| $C4$ | Parameter of $L_{in}$ | **0.552** | **0.225** | **0.604** |
| $C_S$ | Snow exchange coefficient of turbulent heat flux | 0.0038[d] | 0.002[h] | 0.002[h] |
| $C_L$ | Ice exchange coefficient of turbulent heat flux | 0.0038[d] | 0.002[h] | 0.002[h] |
| $\rho_{snow}$ (kg/m$^3$) | Fresh snow density | 200 | 200 | **200** |
| $\rho_{ice}$ (kg/m$^3$) | Ice density | 900 | 900 | 900 |
| $\rho_{firn}$ (kg/m$^3$) | Initial snow density | – | 410 | **410** |
| $T_f$ (ºC) | Fixed bottom temperature at 10 m | **−1.5** | **−4.5** | −3.9[i] |

Bold text indicates parameters in the EMB model that are calibrated using observed data

[a]Optimized using measured values

[b]Calculated using the method of Ma et al. (2015)

[c]Taken from Huintjes et al. (2015)

[d]Taken from Yang et al. (2013)

[e]Taken from Zhu et al. (2015)

[f]Taken from Mölg et al. (2014)

[g]Taken from Wang et al. (2012)

[h]Taken from Fujita and Ageta (2000)

[i]Mean air temperature at AWS2-M

the AWSs were extrapolated to all the grid points on glaciers using a constant altitudinal lapse rate. $T_a$ values at grid points on the three glaciers were created using their respective constant lapse rate. The $T_{rate}$ (−0.38 ºC/100 m) on PL04 glacier was optimized using measurement values (such as net radiation and glacier surface height changes) from AWS2-P and monthly $T_{rate}$ values measured from January 2012 to July 2012 according to data obtained at AWS2-P and AWS3-P. The values of $T_{rate}$, −0.7 ºC/100 m on ZD glacier and −0.67 ºC/100 m on MZ15 glacier, represent measurements. The lowest boundary ice temperature ($T_c$) and depth are listed in Table 3

### 3.4 Model calibration

Comparing model results with field measurements is essential to evaluate the model's ability to capture an accurate surface energy and mass balance. For PL04 glacier, the model is calibrated using data measured over the period 2009–2013 at AWS2-P, and is validated for 2010–2012 using data measured at AWS3-P. Figure 2 shows the modelled and measured values of $\alpha$, $L_{in}$, $T_S$ and stake mass balance at AWS2-P on PL04 glacier. The RMSE between the modelled and observed values of $\alpha$ is 0.14 (Fig. 2a). The discrepancies between the modelled

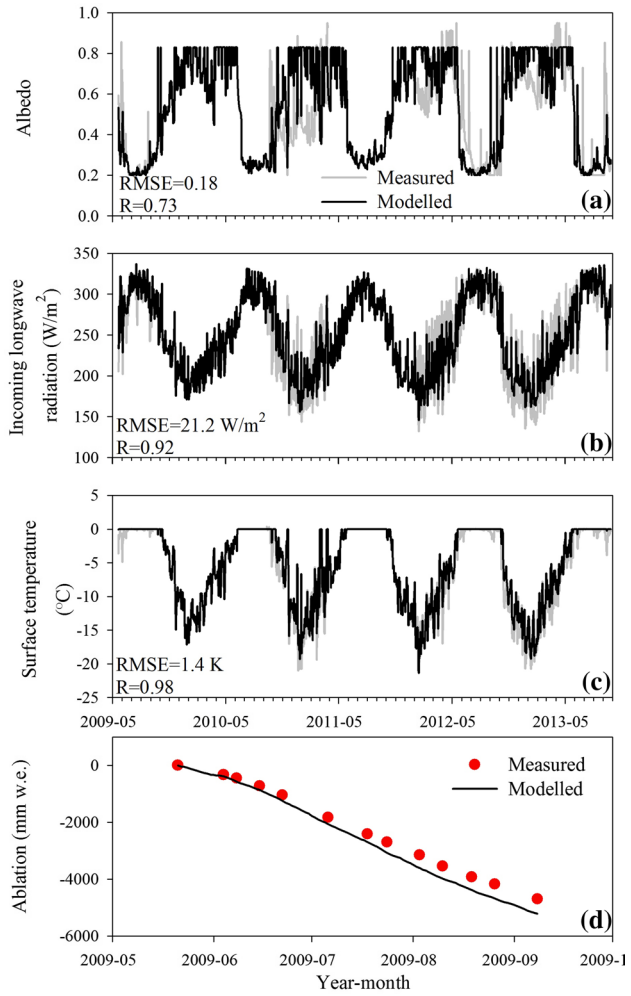


**Fig. 2** Comparisons of simulated results and observations at AWS2-P for PL04 glacier during the observation period, (**a**) daily mean albedo, (**b**) daily mean incoming longwave radiation (positive downward), (**c**) daily mean surface temperature, and (**d**) daily cumulative ablation

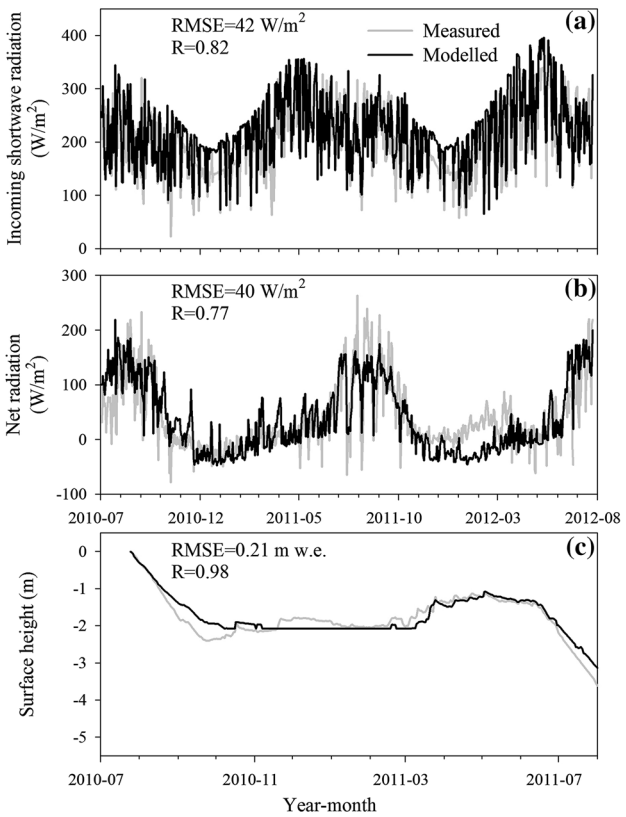


**Fig. 3** Comparisons of simulated results and observations at AWS3-P for PL04 glacier during the observation period; (**a**) daily mean incoming shortwave radiation (positive downward), (**b**) daily mean net radiation, and (**c**) glacier surface height

and observed values of $\alpha$ are found in winter on PL04 glacier, and these discrepancies occur due to the reduction in accumulation caused by snowdrift, resulting in the lower observed value of $\alpha$. However, these discrepancies do not cause substantial error in the calculated mass balance during the ablation season. Therefore, the modelled $\alpha$ values are generally acceptable. The RMSE values are 17.8 W/m$^2$ for $L_{in}$ and 1.4 °C for $T_S$ (Fig. 2b, c). The overall agreement is good, although the modelled variables are somewhat different from the measured values in some periods. Figure 2d shows that the model reproduces the measured mass balance quite well at the site of AWS2-P over the observational period. However, after August 26th, 2009, the cumulative mass balance calculated using the model is slightly larger (0.5 m w.e.) than the measured values.

Figure 3 shows the modelled and measured $S_{in}$ and $R_{net}$ values and surface heights at AWS3-P on PL04 glacier. The RMSE values are 35.5 W/m$^2$ for $S_{in}$ and 41 W/m$^2$ for $R_{net}$. The RMSE of 0.21 m for the glacier surface height changes is a convincing result. The differences in surface heights between the modelled and measured values increase after July 2011, perhaps because of slight tilting of the SR50 mast.

The distance between PL04 glacier and PL94 glacier is only approximate 12 km. In this study, we assume that the mass balance at the same altitude on these two glaciers is the same. We use the stake mass balance at different altitudes on PL94 glacier to verify modelled mass balance on PL04 glacier. Figure 4 shows that the simulated results for PL04 glacier are largely in agreement with the in situ mass balance observation on PL94 glacier for four mass balance years.

For ZD glacier, the model is evaluated at the point scale using observations of $\alpha$, $L_{in}$, $T_s$, $R_{net}$, and surface height taken at AWS1-Z (Fig. 5). The RMSE between the modelled and observed $\alpha$ values is 0.13, and the corresponding R is 0.62 (Fig. 5a). A small discrepancy between the

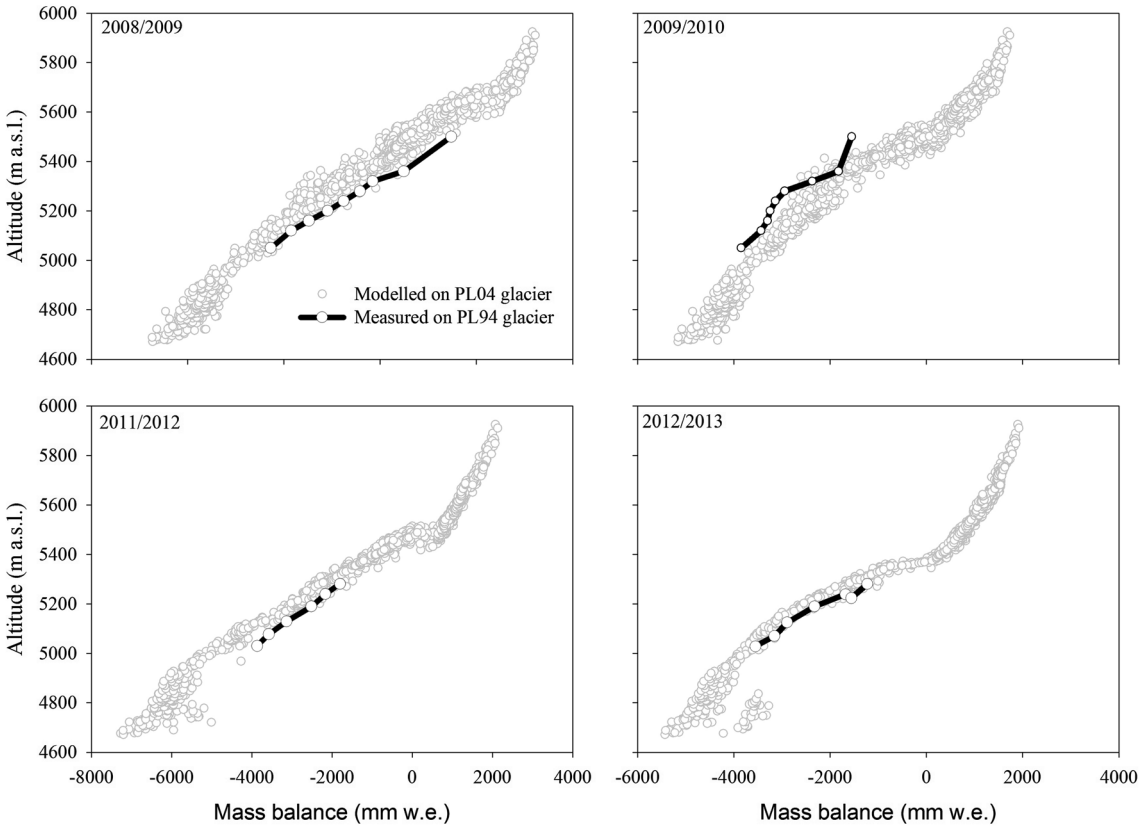


**Fig. 4** Comparison of the modeled annual net mass balance on PL04 glacier and measured annual net mass balance on Parlung94 glacier as a function of elevation in different mass balance years

observed and modelled $\alpha$ occurs after a significant snowfall. The RMSE value is 17.8 W/m$^2$ for $L_{in}$, 2.2 °C for $T_S$ and 32.6 W/m$^2$ for $R_{net}$ (Fig. 5b–d). Figure 5e shows that the model reproduces the measured surface heights quite well. The RMSE between the measured and modelled glacier surface heights is 0.22 m (Fig. 5e).

In addition, the model is evaluated using the stake mass balance for different observational periods, as well as the modelled annual mass balance of the whole glacier, during each balance year. Figure 6a shows the model performance during different observational periods at all stake points. The R value is 0.89, and the RMSE is 300 mm w.e. This is similar to the results from Huintjes et al. (2015), who obtained the R of 0.83 and the RMSE of 340 mm w.e. Figure 6b shows the comparison between the modelled and measured five-year glacier-wide annual mass balance during each balance year. The average bias is 85 mm w.e. a$^{-1}$. On the whole, the agreement between the modelled and measured mass balance values in different years verifies the model's good performance.

For MZ15 glacier, the model was calibrated using the observed mass balance values and snow heights at stakes over the period of 2008–2013 (Fig. 7). Figure 7a describes the model performance during the entire observational period at all of the stake points. The R is 0.87 and the RMSE is 213 mm w.e. Figure 7b compares the simulated and measured five-year annual mass balances during each balance year. The average bias is 43 mm w.e. a$^{-1}$.

We also compared simulated snowpack heights with measurements to further evaluate the robustness of the model for MZ15 glacier. Figure 8 presents the comparison results for the three monitoring stakes at three different altitudes. This comparison reveals that the model can capture the evolution of the snowpack heights. However, the differences between the modelled and measured snow thicknesses increase at higher altitudes. This difference may be a result of snowdrift and the complex nature of refreezing processes. Above all, based on the above analysis, the model primarily captures the surface mass and energy balance on the three glaciers. This result confirms that the model can be further applied to perform analyses of mass balance, energy balance and mass balance sensitivity to climate change.

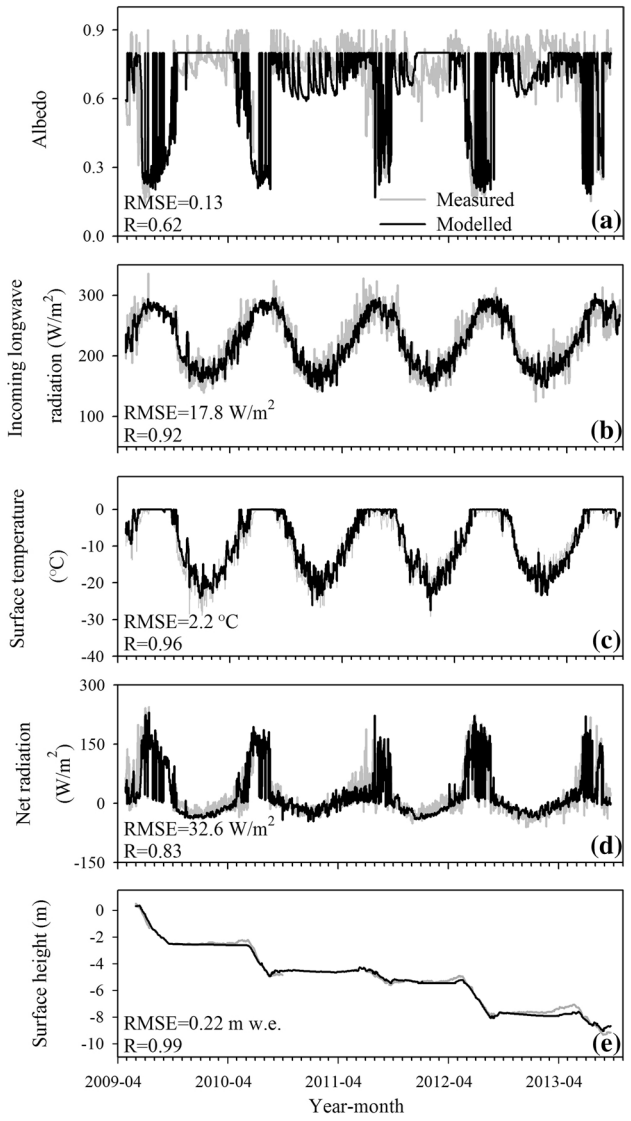


**Fig. 5** Measured (*gray line*) and modelled (*black line*) daily mean albedo (**a**), incoming longwave radiation (**b**), surface temperature (**c**), net radiation (**d**) and surface height (**e**) on ZD glacier during the observation period from April, 2009 to October, 2013

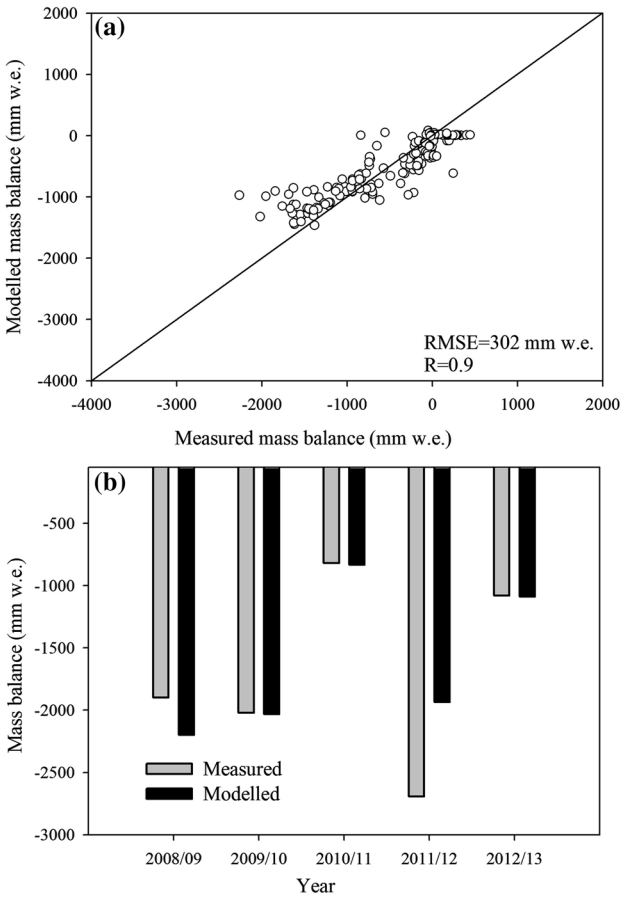


**Fig. 6** Comparison of the modelled and measured mass balance values at stakes (**a**) and on a glacier-wide basis (**b**) on ZD glacier

## 4 Results

This comparative analysis of glacier-wide meteorological characteristics, glacier-wide mass and energy balance and mass balance sensitivity among the three glaciers extended from October 1st, 2008 to September 21st, 2013. The ablation season is defined as from June to September and the cold season extends from October to May.

### 4.1 Meteorological characteristics among the three glaciers

For the three glaciers, monthly mean $T_a$ and *RH* values were higher during the ablation season than during the cold season (Fig. 9a, b). Mean $T_a$ and *RH* values over the entire year and during the cold season were the highest on PL04 glacier, followed by ZD glacier, with the lowest values on MZ15 glacier (Table 4). During the ablation season, the differences in $T_a$ and *RH* between PL04 and ZD glaciers decreased (Fig. 9a, b). $T_a$ and *RH* values were approximately 5 °C and 20% higher on PL04 and ZD glaciers than on MZ15 glacier. In addition, the variations in the monthly mean $T_a$ and *RH* values were smaller on PL04 and ZD glaciers than on MZ15 glacier, perhaps due to the influence of the SAM on PL04 and ZD glaciers (Fig. 9a, b). The annual amplitude of $T_a$ was the lowest on PL04 glacier (15.2 °C), followed by ZD glacier (17.8 °C). The highest amplitude was noted on MZ15 glacier (20.2 °C) (Fig. 9a).

Monthly mean *WS* values were higher during the cold season than during the ablation season for the three

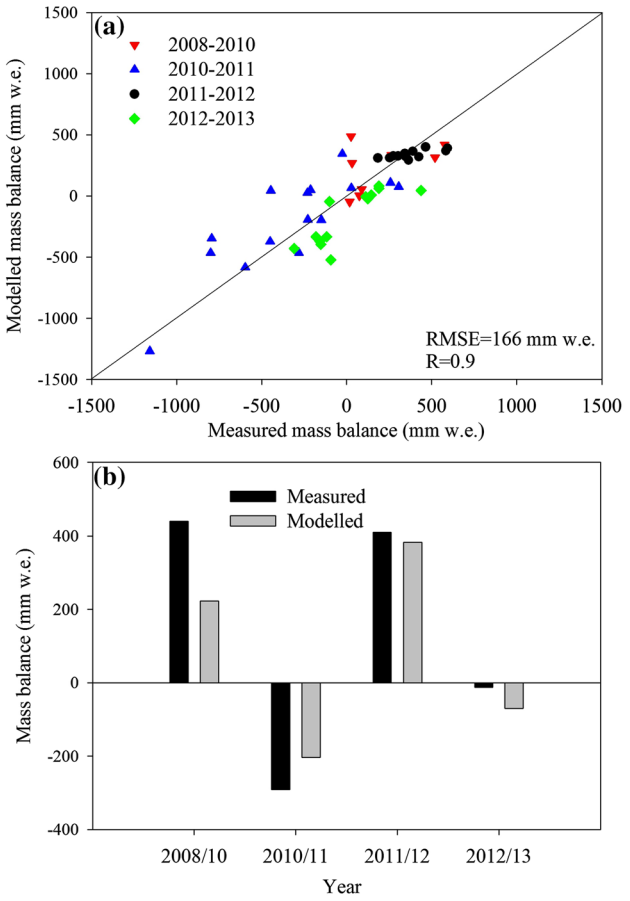


**Fig. 7** Comparison of modelled and measured mass balance values at stakes (**a**) and on a glacier-wide basis (**b**) on MZ15 glacier

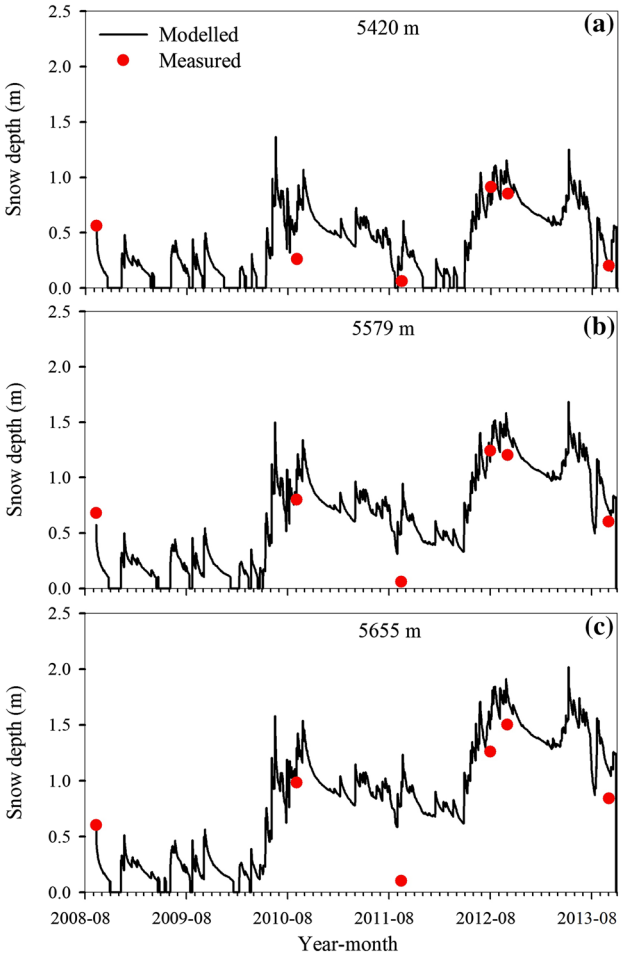


**Fig. 8** Temporal evolution of snow depths simulated using the model (*solid black lines*) and measurements (*red* points) at different altitudes on MZ15 glacier

glaciers (Fig. 9c). Especially for MZ15 glacier, monthly mean *WS* values were significantly higher during the cold season than during the ablation season. Mean *WS* on PL04 and ZD glacier were similar, and their values were approximately 1 and 3 m/s lower than on MZ15 glacier during the ablation and cold seasons, respectively (Table 4).

The change in monthly mean $\tau$ on MZ15 glacier was small, but was large on PL04 and ZD glaciers. On PL04 and ZD glaciers the change of this variable in winter was significantly lower than that in summer (Fig. 9d). The difference in mean $\tau$ among the three glaciers was small during the cold season due to the increased occurrence of clear−sky conditions (Table 4). However, during the ablation season, significant differences occurred in $\tau$ among the three glaciers. The $\tau$ value of PL04 glacier was the smallest, followed by that of ZD glacier, with the largest value from MZ15 glacier. Above all, PL04 and ZD glaciers were characterized by warm, humid, cloudy and low wind conditions, and MZ15 glacier experienced cold, dry, clear and windy conditions.

## 4.2 Comparison of mass balance components on the three glaciers

The three glaciers show significant differences in mass balance (Table 4). Both PL04 and ZD glaciers show strong mass loss, but MZ15 glacier shows a slight mass gain over the whole period and during the ablation season (Table 4). During the cold season, maximum mass balance occurs on PL04 glacier due to the high amount of spring precipitation; the second largest value of mass balance during the cold season occurs on MZ15 glacier, with the minimum on ZD glacier. Glacier mass balance consists of sublimation/evaporation, surface melt, snowfall and refreezing. The details of these components are descripted below.

Sublimation represents an important kind of mass loss. Especially during the cold season, sublimation was the most important factor contributing to mass loss from three glaciers. Table 4 shows that the greatest sublimation occurred on MZ15 glacier during the ablation and

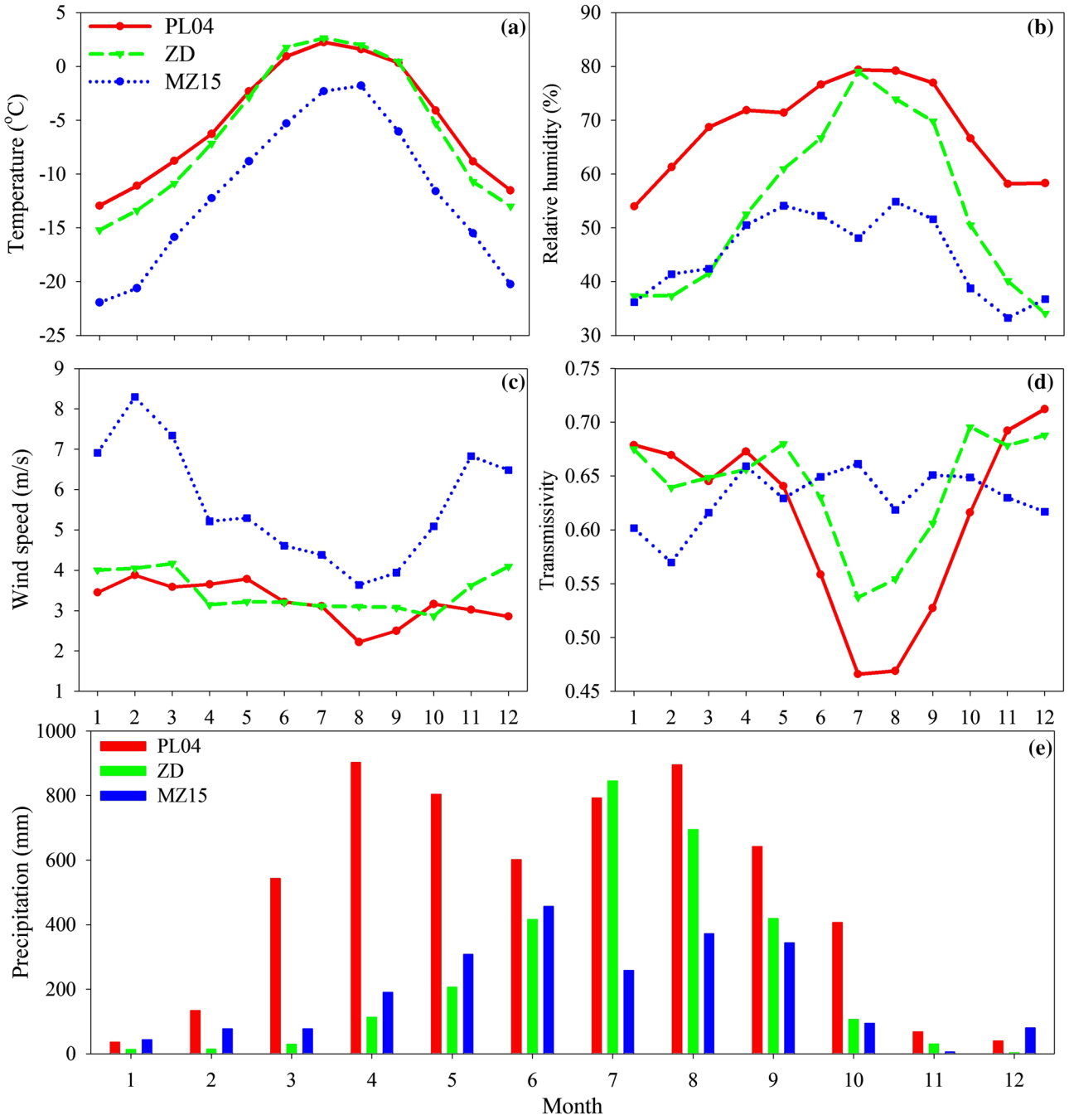


**Fig. 9** Comparison of glacier-wide five-year average monthly air temperature (**a**), relative humidity (**b**), wind speed (**c**), transmissivity (**d**) and precipitation (**e**) from October 2008 to September 2013 on three study glaciers

cold seasons due to the lower values of $T_a$, humidity and larger *WS*. For PL04 and ZD glaciers, sublimation was 1.5 times larger during the cold season than during the ablation season.

Surface melt dominates the mass loss for PL04 and ZD glaciers. It was 9702 and 9164 mm w.e. greater than sublimation on PL04 and ZD glaciers. But for MZ15 glacier, surface melt was 499 mm w.e smaller and 267 mm w.e. larger than sublimation for the whole period and the ablation season, respectively. This result indicates that surface melt and sublimation (or evaporation) are equally important in determining mass balance changes of MZ15 glacier. The differences in surface melt between PL04 and ZD glaciers and MZ15 glacier are enormous. During the ablation season, mass loss caused by surface melt was 9055 and 8761 mm w.e. larger on PL04 and ZD glaciers than

**Table 4** Annual and seasonal mean values of meteorological variables, and annual and seasonal cumulative values of mass balance components

| | PL04 | | | ZD | | | MZ15 | | |
|---|---|---|---|---|---|---|---|---|---|
| | Annual | Ablation season | Cold season | Annual | Ablation season | Cold season | Annual | Ablation season | Cold season |
| Meteorological variables | | | | | | | | | |
| T (ºC) | −5.1 | 1.3 | −8.2 | −6 | 1.7 | −9.8 | −11.9 | −3.9 | −15.9 |
| RH (%) | 69 | 78 | 64 | 54 | 72 | 44 | 45 | 52 | 42 |
| WS (m/s) | 3.2 | 2.8 | 3.4 | 3.5 | 3.1 | 3.6 | 5.6 | 4.1 | 6.4 |
| τ | 0.61 | 0.51 | 0.67 | 0.64 | 0.58 | 0.67 | 0.63 | 0.65 | 0.62 |
| P (mm) | 5870 | 2933 | 2937 | 2897 | 2377 | 520 | 2312 | 1432 | 880 |
| Rain (mm) | 1533 | 1460 | 73 | 407 | 406 | 1 | 26 | 26 | 0 |
| Mass balance components | | | | | | | | | |
| Mass balance (mm w.e.) | −6690 | −8381 | 1691 | −7881 | −7626 | −254 | 342 | 265 | 77 |
| Sublimation/evaporation (mm w.e.) | −724 | −212 | −512 | −772 | −223 | −549 | −1360 | −568 | −792 |
| Surface melt (mm w.e.) | 10,395 | 9914 | 481 | 9936 | 9620 | 316 | 793 | 782 | 11 |
| Snowfall (mm w.e.) | 4337 | 1473 | 2864 | 2490 | 1971 | 519 | 2286 | 1406 | 880 |
| Refreezing (mm w.e.) | 548 | 335 | 213 | 337 | 246 | 92 | 209 | 209 | 0 |

$\tau$ transmissivity

that on MZ15 glacier. During the cold season, especially in May and October, small amounts of surface melt occur on PL04 and ZD glaciers, but no surface melt takes place on MZ15 glacier. The difference in the change in surface melt between PL04 and ZD glaciers and MZ15 glacier during the ablation season are close to that of the annual mass balance.

Mass gain is mainly due to snowfall on the three glaciers (Table 4). During the ablation season, the amounts of snowfall recorded on MZ15 and PL04 glaciers were 565 and 498 mm less than that on ZD glacier, respectively. During the cold season, almost all the *P* fell as snow on the three glaciers. Snowfall amounts were 2864, 519 and 880 mm w.e. on PL04, ZD and MZ15 glaciers, respectively. Seasonal distributions of snowfall differed among the three glaciers. *P* mainly occurred in spring and summer on PL04 glacier (Fig. 9e). On this glacier, snowfall was 1.9 times greater during the cold season than during the ablation season because higher $T_a$ values led to unfavorable conditions for snowfall during the ablation season. Therefore, PL04 glacier shows spring accumulation features. For ZD glacier, which is characterized by summer accumulation types, 79% of total snowfall and 82% of total *P* occurred during the ablation season (Fig. 9e; Table 4). For MZ15 glacier, 62% of total snowfall and 62% of total *P* occurred during the ablation season, but snowfall amount was only 537 mm w.e. greater during the ablation season than during the cold season (Table 4). Snowfall and *P* during the ablation season and the cold season are equally important for MZ15 glacier. In addition, snowfall and *P* during the cold season mainly occurred in April and May (Fig. 9e). Thus, MZ15 glacier displays both spring and summer accumulation features.

We also incorporated into the modelled a given amount of meltwater refrozen into the snowpack, which is an important form of englacial mass storage on the three glaciers. The difference in the amount of refreezing is small among the three glaciers (Table 4). The refrozen amount on PL04 glacier is the highest, resulting from high surface melt and the thick snowpack observed on this glacier (Table 4). The amount of refreezing is lowest on MZ15 glacier, but the ratio of the amount of refreezing and the meltwater is the highest. On MZ15 glacier, 26% of the meltwater was refrozen within the snowpack and this percentage was larger than that on PL04 glacier (5.4%) and ZD glacier (4.0%). This ratio on MZ15 glacier was similar to the value (20%) on Xiao Dongkemadi glacier, which is located on the central TP (Fujita and Ageta 2000). This discrepancy in the ratio among these glaciers can be partly attributed to the different climate settings of these glaciers.

Overall, PL04 glacier is characterized by high melt and accumulation. ZD glacier presents characteristics of high melt and low accumulation. MZ15 glacier shows low melt, high sublimation and low accumulation. The significant differences in mass balance that occur between PL04 and ZD glaciers and MZ15 glacier mainly result from variations in surface melt during the ablation season.

### 4.3 Comparison of energy balance fluxes on the three glaciers

For the three glaciers, during both the ablation and cold seasons, $S_{in}$ and $L_{in}$ dominated energy input, followed by $H_{sen}$. $L_{out}$, $H_{lat}$, $Q_M$ and $Q_G$, leading to the development of an energy sink at the glacier surface (Table 5; Fig. 10). Compared to the cold season, a significant increase of $S_{in}$ and $L_{in}$ occurred during the ablation season, resulting in glacier melt during the ablation season. The detailed features of the energy balance components are described below.

Figure 10a shows monthly mean $S_{in}$ values on the three glaciers. The seasonal distribution of $S_{in}$ on PL04 glacier is similar to that on ZD glacier but differs from that on MZ15 glacier. The largest $S_{in}$ values on PL04 and ZD glaciers appeared in May due to the increase in cloud cover associated with the onset of the SAM. The largest $S_{in}$ value on MZ15 glacier occurred in July. In addition, the differences in $S_{in}$ among the three glaciers were significant during the ablation season (Table 5). These differences in $S_{in}$ are caused by cloud cover, not by the latitude (Table 2). The differences in $S_{in}$ among the three glaciers were small during the cold season due to the combined impact of the latitude of the sites and cloud cover. The distribution of $S_{in}$ at the three sites was contrary to that of the melt energy on the three glaciers during the ablation season; therefore, $S_{in}$ does not cause the difference in melt energy on the three glaciers.

Vast differences in $S_{out}$ appeared among the three glaciers during the ablation season, especially between MZ15 glacier on the one hand and PL04 and ZD glaciers on the other (Table 5; Fig. 10b). Compared to MZ15 glacier, the absolute values of $S_{out}$ are 91 W/m$^2$ and 76 W/m$^2$ smaller on PL04 and ZD glaciers, respectively. The largest and smallest differences in monthly mean $S_{out}$ between PL04 and ZD glaciers and MZ15 glacier occurred in July and in September, respectively. During the cold season, the difference in $S_{out}$ among the three glaciers was relatively small. The largest difference in the mean value of $S_{out}$ between PL04 and MZ15 glaciers was only 18 W/m$^2$. The distribution of $S_{out}$ among the three glaciers is in agreement with that of melt energy during the ablation season. $S_{out}$ is important for differentiation of the melt energy on the three glaciers.

$L_{in}$ was another important energy source for surface melt on the three glaciers. During both the ablation and cold seasons, the largest values of $L_{in}$ occurred on PL04 glacier, with the next largest value associated with ZD glacier, and the smallest value associated with MZ15 glacier (Table 5). The monthly mean $L_{in}$ value was 61–73 W/m$^2$ larger on PL04 glacier and 41–53 W/m$^2$ larger on ZD glacier than that on MZ15 glacier during the ablation season (Fig. 10c). The differences in mean $L_{in}$ among the three glaciers were smaller during the cold season than those that occurred during the ablation season.

$L_{out}$ was the largest energy sink on the three glaciers. The differences in $L_{out}$ among the three glaciers were relatively small during the ablation season. The values of $L_{out}$ on PL04 and ZD glaciers are close to each other due to the continuous occurrence of surface melt during the ablation season (Table 5; Fig. 10d). Compared to PL04 and ZD

**Table 5** Seasonal mean values of energy-flux components (W/m$^2$)

| | PL04 | | | ZD | | | MZ15 | | |
|---|---|---|---|---|---|---|---|---|---|
| | Mean | Ablation season | Cold season | Mean | Ablation season | Cold season | Mean | Ablation season | Cold season |
| Sin | 213 | 211 | 214 | 202 | 238 | 184 | 223 | 288 | 191 |
| α | 0.64 | 0.56 | 0.68 | 0.66 | 0.56 | 0.71 | 0.69 | 0.73 | 0.66 |
| Sout | −136 | −118 | −145 | −133 | −133 | −131 | −154 | −209 | −127 |
| Snet | 77 | 93 | 69 | 69 | 105 | 53 | 69 | 79 | 64 |
| Lin | 242 | 291 | 217 | 229 | 278 | 204 | 196 | 233 | 177 |
| Lout | −288 | −314 | −275 | −278 | −314 | −260 | −257 | −288 | −241 |
| Lnet | −46 | −23 | −58 | −49 | −36 | −56 | −61 | −55 | −64 |
| Rnet | 31 | 70 | 11 | 20 | 69 | −3 | 8 | 24 | 0 |
| Hsen | 11 | 13 | 10 | 14 | 9 | 17 | 18 | 14 | 20 |
| Hlat | −21 | −14 | −24 | −13 | −11 | −14 | −24 | −31 | −21 |
| QG | 1 | −7 | 5 | −1 | −6 | −1 | 0 | −2 | 1 |
| QPS | −5 | −8 | −4 | −4 | −7 | −3 | −1 | −1 | −1 |
| G | 6 | 1 | 9 | 3 | 1 | 4 | 1 | −1 | 2 |
| QM | −22 | −62 | −2 | −20 | −61 | −1 | −2 | −5 | 0 |

*α* albedo, *Lnet* net longwave radiation, $H_{sen}$ sensible heat flux, $H_{lat}$ Latent heat flux, *QG* subsurface heat flux, *OPS* penetrating shortwave radiation, *G* conductive heat flux, $Q_M$ melt energy

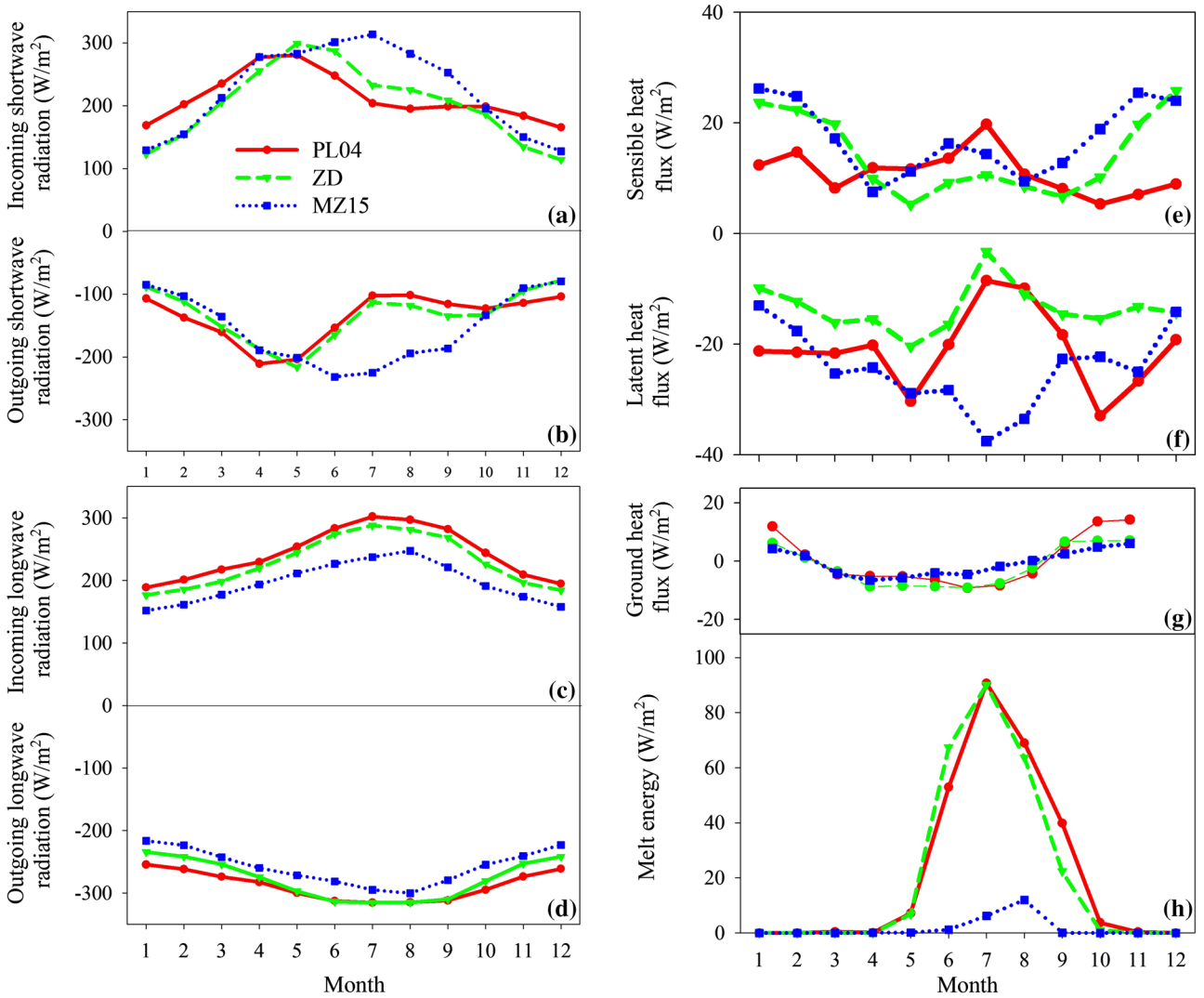


**Fig. 10** Comparison of glacier-wide five-year average monthly incoming shortwave radiation (**a**), outgoing shortwave radiation (**b**), incoming longwave radiation (**c**), outgoing longwave radiation (**d**), sensible heat flux (**e**), latent heat flux (**f**), ground heat flux (**g**) and melt energy (**h**) from October 2008 to September 2013 on three study glaciers

glaciers, the absolute value of $L_{out}$ on MZ15 glacier was only 23 W/m$^2$ lower. Thus, less surface melt occurred on MZ15 glacier. During the cold season, the largest absolute value of $L_{out}$ was associated with PL04 glacier, the next largest value was found for ZD glacier, and the smallest value was for MZ15 glacier. In general, smaller $L_{out}$ values mean that more energy is used to melt glacier ice. Thus, the different values of $L_{out}$ do not lead to the differences in $Q_M$ between PL04 and ZD glaciers and MZ15 glacier.

The contribution of turbulent heat flux to $Q_M$ was relatively small (Table 5; Fig. 10e, f). $H_{sen}$ was only 4 W/m$^2$ larger on PL04 glacier and 5 W/m$^2$ larger on MZ15 glacier than that on ZD glacier during the ablation season, because larger temperature differences existed between the air and the glacier surface on PL04 and MZ15 glaciers. During the cold season, $H_{sen}$ was largest on MZ15 glacier, the next largest value was associated with ZD glacier, and the smallest value occurred on PL04 glacier. The absolute value of $H_{lat}$ was 18 and 20 W/m$^2$ smaller on PL04 and ZD glaciers than on MZ15 glacier during the ablation season because of lower specific humidity and higher *WS* that occur on MZ15 glacier. The high $H_{lat}$ values associated with MZ15 glacier indicate that large amounts of sublimation occur there. High sublimation facilitates the survival of MZ15 glacier by consuming more energy that would otherwise be available for surface melt (Nicholson et al. 2013; Wagnon et al. 1999). During the cold season, the absolute value of $H_{lat}$ was largest on PL04 glacier, followed by MZ15 glacier, with the smallest value was associated with ZD glacier.

Compared with other energy fluxes, $Q_G$ was the smallest (Fig. 10g; Table 5). The absolute value of $Q_G$ was below 7 W/m$^2$ during the ablation season and below 5 W/m$^2$ during the cold season on the three glaciers. $Q_G$ consists of *QPS* and *G*. The mean *QPS* values were close to each other on PL04 and ZD glaciers, and these values were approximately 6 W/m$^2$ less during the ablation season and 2 W/m$^2$ less during the cold season than the values associated with MZ15 glacier. During the ablation season, *G* was always above 0 on PL04 and ZD glaciers, which means that heat is transferred from underground to warm the glacier surface. In contrast, *G* was negative on MZ15 glacier, reflecting its nature as a continental glacier. During the cold season, the value of *G* was largest on PL04 glacier. The next largest value occurred on ZD glacier, with the smallest value from MZ15 glacier.

The values of $Q_M$ were close to each other on PL04 and ZD glaciers, but there was a significant difference between PL04 and ZD glaciers and MZ15 glacier (Fig. 9h). Especially during the ablation season, compared to MZ15 glacier, the values of $Q_M$ were 57 and 56 W/m$^2$ larger on PL04 and ZD glaciers (Table 5). Surface melt occurs from April to October on PL04 and ZD glaciers and from June to September on MZ15 glacier (Fig. 10f). The maximum value of $Q_M$ appeared in July on PL04 and ZD glaciers, which is in agreement with the results of Li et al. (2016), and appeared in August on MZ15 glacier. During the cold season, the mount of $Q_M$ was slightly larger on PL04 and ZD glaciers than that on MZ15 glacier. Because surface melt occurred sporadically in May and October on PL04 and ZD glaciers, but no melt occurred on MZ15 glacier.

Above all, during the ablation season, melt energy showed both significant differences between MZ15 and PL04 glaciers, and between MZ15 and ZD glaciers. The differences in $S_{out}$ and $L_{in}$ between PL04 and ZD glaciers and MZ15 glacier brought about this differentiation. In addition, $H_{lat}$ also contributed to the differences in melt energy between PL04 and ZD glaciers and MZ15 glacier.

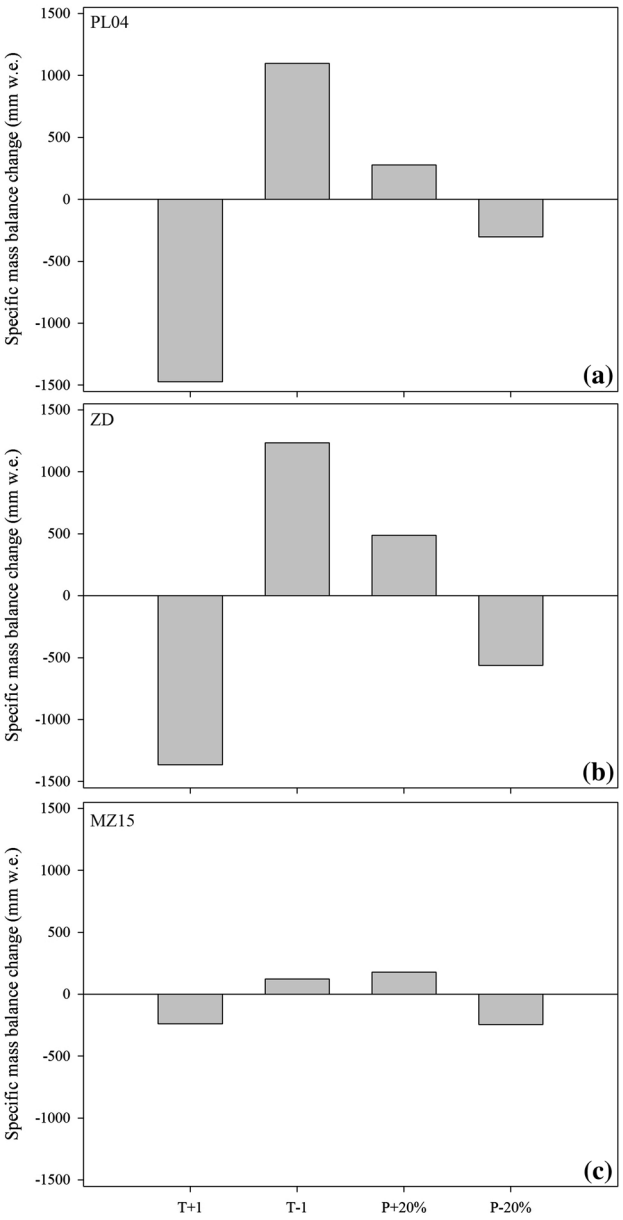


**Fig. 11** Sensitivity of the mass balance of PL04, ZD and MZ15 glaciers to changes in air temperature and precipitation

### 4.4 Mass balance sensitivity on the three glaciers

The sensitivity of glaciers to climatic change is key to assessing the differences in the response to climate change for the three glaciers. The mass balance sensitivity to $T_a$ change and *P* change were calculated using the method proposed by Oerlemans et al. (1998). The sensitivity analysis was carried out by performing a model run with perturbed conditions for step wise changes of +1 and −1 °C in $T_a$ and +20 and −20% changes in *P* (Mölg et al. 2008; Zhang et al. 2013) from October 2008 to September 2013. Figure 11 shows the calculated sensitivities of the mass balance for the three glaciers.

Both PL04 and ZD glaciers showed higher sensitivities to $T_a$ change (1283 and 1300 mm w.e. a$^{-1}$ °C$^{-1}$) than MZ15 glacier (181 mm w.e. a$^{-1}$ °C$^{-1}$). The sensitivities of mass balance to *P* change were 292, 524 and 210 mm w.e. a$^{-1}$ (20%)$^{-1}$ on PL04, ZD and MZ15 glaciers, respectively. Mass balance sensitivity to $T_a$ change and *P* change on PL04 glacier was consistent with those on PL94 glacier (Fig. 8 in Yang et al. 2013). In this study, mass balance sensitivity to $T_a$ change on ZD glacier is comparable to the value of 1150 mm w.e. a$^{-1}$ °C$^{-1}$ obtained by Li et al. (2015) and is higher than the value of 470 mm w.e. a$^{-1}$ °C$^{-1}$ obtained by Mölg et al. (2012). In addition, mass

balance sensitivity to $P$ change (260 mm w.e. $a^{-1}$ $(10\%)^{-1}$) is slightly higher than results of Mölg et al. (2012) (140 mm w.e. $a^{-1}$ $(10\%)^{-1}$). Mass balance sensitivity to $T_a$ change obtained for MZ15 glacier in this study lies within the range of values (170 to 470 mm w.e. $a^{-1}$ $°C^{-1}$) found for glaciers in the Tianshan mountains (Rasmussen 2013), which lie near the Muztag Ata region. In addition, it is obvious that mass balances of PL04 and ZD glaciers were more sensitive to a 1 °C change in $T_a$ than to a 20% change in $P$. However, for MZ15 glacier, mass balance was slightly more sensitive to a 20% change in $P$ than to a 1 °C change in $T_a$ (Fig. 11). In particular, mass balance sensitivities to $T_a$ change and $P$ change were higher on PL04 and ZD glaciers than on MZ15 glacier, especially mass balance sensitivity to $T_a$ change.

## 5 Discussion

### 5.1 Uncertainty analysis of mass balance calculations

The parameters of the EMB model were obtained from observations or taken from the literature (Table 3). The parameters show different values on the three glaciers, especially for $T_{rate}$, precipitation lapse rate ($P_{rate}$) and air temperature thresholds for rain ($T_{rain}$). Guo et al. (2016) found different values of $T_{rate}$ and $P_{rate}$ in the different regions within and around the TP. For example, the observed $T_{rate}$ was found to vary from −0.46 to −0.73 °C/100 m in the different regions of the TP, and the spatial variability of $T_{rate}$ was found to be related to climate conditions; $T_{rate}$ increases under dry conditions and in cold months (October–April), whereas it diminishes in humid regions and during warm months (May–September) (Guo et al. 2016). For valley glaciers, $T_{rate}$ differs among the different parts of individual glaciers (Ayala et al. 2015; Greuell and Böhm 1998). Even positive off-glacier temperatures generate katabatic effects that result in positive $T_{rate}$ over the upper sections of glaciers (Ayala et al. 2015). Significant katabatic winds occur on PL04 glacier (Yang et al. 2011), which causes lower absolute value of $T_{rate}$. In addition, Ding et al. (2014) argued that precipitation types were highly dependent on surface elevation and humidity. A higher threshold temperature is needed to differentiate snow and rain over high-elevation regions, and the probability of sleet events rises greatly with an increase in relative humidity (Ding et al. 2014). Thus, $T_{rain}$ varies among the different regions of the TP because of differences in climate and terrain.

Sensitivity analyses of parameters, in which input parameter values are changed systematically, can be used to test the reliability of model results. In this study, the parameters of the EMB model were obtained either from observations made at glaciers or were adopted from the literature. The formulations used in the model contain several unknown or poorly constrained parameters. Previous work has shown that model results can be greatly influence by uncertain input parameters, including the parameters used in parameterizations of $\alpha$, the parameters used in parameterizations of turbulent heat fluxes, the $T_{rate}$, the $P_{rate}$, the $T_{snow}$ and the $T_{rain}$ (Giesen et al. 2008; Hock and Holmgren 2005; Mölg and Hardy 2004; Reijmer and Hock 2008; Zhu et al. 2015). In the following analysis, we performed a sensitivity test of parameters used in the EMB model by changing the input parameter values (Table 6).

For the three glaciers, the high sensitivity of the parameters is related to snow albedo ($a_{snow}$) in the $\alpha$ model. When the $a_{snow}$ value is increased (or decreased) by 10%, a mass gain (or loss) of 977 (or 1236), 4599 (or 3016), and 557 (or

**Table 6** Sensitivity of glacier-wide cumulative mass balance (mm w.e.) to parameter changes over the period from October 1st, 2008 to September 21st, 2013

| Parameter | Perturbation | Total mass balance change | | |
|---|---|---|---|---|
| | | PL04 | ZD | MZ15 |
| Reference | 0 | −6690 | −7881 | 342 |
| $a_{snow}$ | 10% | 977 | 4599 | 557 |
| | −10% | −1236 | −3016 | −812 |
| $a_{firn}$ | 10% | 507 | 603 | 322 |
| | −10% | −448 | −593 | −334 |
| $a$ | 10% | 65 | 254 | 64 |
| | −10% | −69 | −285 | −57 |
| $b$ | 10% | 347 | 430 | 47 |
| | −10% | −340 | −445 | −45 |
| $t^*$ | 10% | 139 | 131 | 100 |
| | −10% | −145 | −143 | −99 |
| $d^*$ | 10% | −20 | −176 | −42 |
| | −10% | 19 | 171 | 48 |
| $C_S$ | 10% | −30 | −132 | −153 |
| | −10% | 32 | 132 | 162 |
| $C_L$ | 10% | −96 | −53 | 10 |
| | −10% | 97 | 50 | −4 |
| $T_{rate}$ | 10% | 1239 | 66 | 455 |
| | −10% | −1423 | −70 | −740 |
| $P_{rate}$ | 10% | 472 | 68 | 252 |
| | −10% | −478 | −68 | −251 |
| $T_{snow}$ | 0.5 | 403 | 623 | 45 |
| | −0.5 | −370 | −654 | −38 |
| $T_{rain}$ | 0.5 | 987 | 166 | 82 |
| | −0.5 | −1147 | −192 | −69 |

$a_{snow}$ fresh snow albedo, $a_{firn}$ firn snow albedo, $a$ parameter of ice albedo, $b$ parameter of ice albedo, $t^*$ albedo time scale, $d^*$ albedo depth scale, $C_S$ snow exchange coefficient of turbulent heat flux, $C_L$ ice exchange coefficient of turbulent heat flux, $T_{rate}$ vertical air temperature gradient, $P_{rate}$ vertical precipitation gradient, $T_{snow}$ phase threshold for snow, $T_{rain}$ phase threshold for snow

812) mm w.e. occurred on PL04, ZD, and MZ15 glaciers, respectively. In addition, variations in firn albedo ($a_{firn}$) also significantly affected the mass balances of these three glaciers. The sensitivity to $a_{snow}$ change and $a_{firn}$ change is higher because shortwave radiation provides more than 50% of the melt energy for these three glaciers. Calibration of the $a_{snow}$ and $a_{firn}$ using values measured on PL04 and ZD glaciers could reduce the uncertainty of the model. For the other parameters of the $\alpha$ model, their changes have small effects on the mass balance of these three glaciers.

Mass balance is insensitive to the change of the transfer coefficients of turbulent heat flux for snow ($C_S$) and ice ($C_L$). A change of 10% resulted in a mass balance change of less than 150 mm w.e. for PL04 and ZD glaciers. The low sensitivity to $C_S$ and $C_L$ is a result of the low values of $H_{sen}$ and $H_{lat}$ on PL04 and ZD glaciers. MZ15 glacier showed a little higher sensitivity to $C_S$ change than was seen on PL04 and ZD glacier due to the larger amounts of sublimation that occurred in MZ15 glacier and that glacier's long period of snow cover.

Mass balance shows a high sensitivity to $T_{rate}$ change on PL04 and MZ15 glaciers and low sensitivity on ZD glacier. This result is consistent with that of Li et al. (2014), who found that mass balance was insensitive to $T_{rate}$ change on ZD glacier. For PL04 and MZ15 glaciers, changing $T_{rate}$ significantly affected $L_{in}$, turbulent heat fluxes, and $\alpha$, and furthermore causes mass balance changes. The sensitivity of mass balance to $P_{rate}$ change was higher on PL04 and MZ15 glaciers than on ZD glacier because the change in $\alpha$ and snowfall caused by the variation in $P_{rate}$ was larger on PL04 and MZ15 glaciers. In fact, both $T_{rate}$ and $P_{rate}$ on PL04 and MZ15 glaciers and $T_{rate}$ on ZD glacier were determined from field measurements, which could reduce the uncertainty of the model results.

Changes in $T_{snow}$ and $T_{rain}$ result in variations in snowfall, alter the energy fluxes through changing $\alpha$ and finally lead to changes in glacier mass balance. $T_{snow}$ and $T_{rain}$ have different effects on mass balance changes for the three glaciers. For PL04 glacier, its mass balance was highly sensitive to $T_{rain}$ change. For ZD glacier, its mass balance is highly sensitive to $T_{snow}$ change. But for MZ15 glacier, variations in $T_{snow}$ and $T_{rain}$ had little impact on mass balance because of almost all of the precipitation falls as snow, even if $T_{snow}$ and $T_{rain}$ increased or decreased. To reduce the uncertainty of the model results, the value of $T_{rain}$ on PL04 glacier and $T_{snow}$ on ZD glacier were obtained from previous studies (Mölg et al. 2012; Yang et al. 2013), in which these parameters are determined through optimization.

In the model, the lack of a parameterization of snow drift result in unavoidable biases in the final results. Especially in winter, strong winds lead to significant snow drifting on the three glaciers. The blowing-snow process increase the moisture content of the near-surface atmosphere so much that it is close to saturation, which is opposite of surface sublimation (Barral et al. 2014). In addition, Bintanja and Reijmer (2001) also found that blowing snow increases the water vapor content within this suspension layer, tends to saturate the near-surface layers (up to a height of 18 cm in the strongest recorded winds) and causes a lowering of the vertical moisture gradient at the surface and a reduction in surface sublimation. However, this reduction in surface sublimation by snow drift is not calculated in the EMB model. Therefore, surface sublimation is overestimated in the EMB model (Barral et al. 2014; Huintjes et al. 2015), ultimately leading to an underestimation of the mass balance for the three glaciers during the cold season. In addition, the blowing-snow process is not only an important factor in determining the spatial variability of snow accumulation and ablation, but also affects the energy budget of the snowpack (Barral et al. 2014; Huintjes et al. 2015). Unfortunately, snow drift processes are very complex, and they could not be accurately modelled due to the lack of in situ measurements from the three glaciers. In this study, we did not directly analyze the effects of snow drift on the mass-energy balance process; instead, we account for these effects by calibrating the model parameters.

The uncertainties for PL04 and ZD glaciers can be limited to a small scope because more measured data can be used in the model, especially for $\alpha$ and $T_{rate}$. However, for MZ15 glacier, the uncertainties associated with $a_{snow}$, $a_{firn}$ and $C_S$ are difficult to avoid due to the lack of measurements. The overall ranges of uncertainties were calculated by combining the major contributors to the uncertainty derived individually from the sensitivity analysis of the parameter (not calibrated using measured values) according to the standard law of error propagation. The parameters which were not calibrated using measured values were selected to calculate the overall range of uncertainty. For PL04 glacier, the selected parameters were $C_S$, $C_L$, $T_{rate}$, $T_{snow}$, and $T_{rain}$. For ZD glacier, the selected parameters were $C_S$, $C_L$, $P_{rate}$, $T_{snow}$, and $T_{rain}$. For MZ15 glacier, the selected parameters were $a_{snow}$, $a_{firn}$, $a$, $b$, $t^*$, $d^*$, $C_S$, $C_L$, $T_{snow}$, and $T_{rain}$. Each parameter, when modified, provided two new 5-year series of annual mass balance, one shifted toward negative values and the second shifted toward positive values. Thus, the uncertainty derived from the parameter sensitivity analysis, which employs two values per parameter, and the absolute value of the uncertainty, which is larger, was used to calculate the overall range of the uncertainty. The overall uncertainty ranges were ±375 mm w.e. $a^{-1}$, ±140 mm w.e. $a^{-1}$ and ±180 mm w.e. $a^{-1}$ for PL04, ZD and MZ15 glaciers, respectively. It should be noted that such uncertainty analysis only covers some factors and some reasonable ranges for some parameters in the model. There are other uncertainties due to model internal features, such as snowdrift, deficient albedo

parametrizations or even theoretical deficits in the current generation of melt models (for example with respect to the bulk approach (Radić et al. 2017)). Thus, the errors might be larger than what is apparent from their sensitivity analysis.

In 2011–2012, the modelled mass balance was very different from measured mass balances on ZD glacier. A detailed analysis of the simulated mass/energy components and in situ measurements of the meteorological variables reveal that this underestimation is linked to the abnormal underestimation of surface melt that occurred in the ablation season of 2012. From the physical energy-mass perspective, net shortwave radiation ($S_{net}$) is the dominant energy source during the ablation season on ZD glacier (Zhang et al. 2013; Zhu et al. 2015). The high simulated surface albedo during the ablation season should be the main reason for this mass balance underestimation. Actually, $\alpha_{fresh}$ is not constant and varies seasonally (Zhang et al. 2013). Fujita and Sakai (2014) found that $\alpha_{fresh}$ was affected by air temperature. The high $T_a$ in 2011–2012 led to a low $a_{snow}$, which was not considered in the model. Admittedly, snow and ice albedo parameterization represents an important challenge in current glaciological studies. Thus, such empirical albedo parameterization methods need to be further improved from the physical perspective in our future work. Although differences between the modelled and measured mass balances on MZ15 glacier were larger in the year 2008–2010 (Fig. 7), these differences were the sum of errors in two years (2008–2009 and 2009–2010). These differences were smaller than the upper boundary of the uncertainty range obtained from the EMB model on MZ15 glacier.

### 5.2 The spatial differences in melt energy and their links to the spatial pattern of Tibetan glacier mass balance changes

The differences in melt, which are mainly driven by $L_{in}$ and $S_{out}$, lead to the discrepancy in the mass balance of MZ15 and PL04 and ZD glaciers during the ablation season. $L_{in}$ and $S_{out}$ should be related to the spatial pattern of Tibetan glacier changes. $L_{in}$ and $S_{out}$ from the HAR30 were used to analyze the spatial relationships between $L_{in}$, $S_{out}$ and the mass balance changes on the TP. Figure 12 shows the spatial distribution of mean $L_{in}$, $S_{out}$ and $L_{in}$+$S_{out}$ during the ablation season on and around the TP from 2001 to 2013. The index $L_{in}$+$S_{out}$ was used to represent the combined influence of $L_{in}$ and $S_{out}$ on mass balance changes.

$L_{in}$ decreased and the absolute value of $S_{out}$ increased from the southeastern portion of the TP to the northwestern portion of the TP and from the Himalaya mountains to the inner TP (Fig. 12a, b). The high values of $L_{in}$+$S_{out}$ occurred in the southern TP and the Himalaya mountains, which are influenced by the SAM, and occurred also in the Qilian mountains and Tianshan mountains (except for the central Tianshan mountains), which are influenced by the westerlies (Fig. 12c). In these areas, glacier mass losses were larger than those found on glaciers in other parts of the TP during the period 2003s–2010s (Farinotti et al. 2015; Kääb et al. 2015; Neckel et al. 2014; Yao et al. 2012). In addition, for the Qilian mountains, glacier mass losses in the eastern part of the range were larger than those in the western part due to higher $L_{in}$ and lower $S_{out}$ values in the eastern part. The mass balance of Ningchanhe No.1 glacier (−1260 mm w.e. $a^{-1}$) in the eastern Qilian mountains was larger than that of Qiyi glacier (about −417 mm w.e. $a^{-1}$) in the western Qilian mountains during the period 2010–2012 (Cao 2013; Wang et al. 2017). This conclusion is also verified by glacier area changes observed in the eastern and western parts of the Qilian mountains (Tian et al. 2014). Low values of $L_{in}$+$S_{out}$ appear in the Karakoram mountains, the eastern Pamir and the western Kunlun mountains, where glacier mass balance was slightly negative or even positive during the period 2003s–2010s (Gardner et al. 2013; Kääb et al. 2015; Neckel et al. 2014; Yao et al. 2012).

What resulted in the spatial differences in $L_{in}$ and $S_{out}$ on the TP? The spatial distribution of $L_{in}$ and $S_{out}$ are related to local climatic factors, such as $T_a$, humidity, $P$ and cloudiness. In addition, atmospheric circulation also has an indirect influence on $L_{in}$ and $S_{out}$ through changes in local climatic factors, such as $T_a$ or $P$. It has been recognized that $L_{in}$ is mainly influenced by $T_a$, humidity, and cloudiness, according to published parameterizations of $L_{in}$ (Crawford and Duchon 1999; Sicart et al. 2011). Compared to MZ15 glacier, $T_a$, humidity and cloudiness were higher on PL04 and ZD glaciers, which lead to larger values of $L_{in}$ on these two glaciers. In addition, the SAM also contributes to the occurrence of larger $L_{in}$ values on PL04 and ZD glaciers because it brings more cloud cover and warm moist air to the southern TP. Especially during the onset in June and the cessation in September of the SAM (Mölg et al. 2012), $L_{in}$ increases faster and decreases slower on glaciers within the monsoon region than on glaciers in the westerly region. The differences in $L_{in}$ between May and June were 31, 30 and 14 W/m$^2$ on PL04, ZD and MZ15 glaciers, respectively. In addition, differences in $L_{in}$ between August and September were −16, −14 and −26 W/m$^2$ on PL04, ZD and MZ15 glaciers, respectively.

$S_{out}$ is influenced by $S_{in}$ and $\alpha$; however, only the spatial distribution of $\alpha$ was consistent with that of $S_{out}$ for these three glaciers, so $\alpha$ mainly contributes to the differences in $S_{out}$. $\alpha$ is primarily governed by snowfall (Favier et al. 2004; Huintjes 2014), and it is related to $T_a$ during the ablation season, $P$ and melt energy. The high $T_a$ values noted for PL04 and ZD glaciers resulted in decreases in snowfall and high $L_{in}$ and turbulent heat fluxes during the ablation

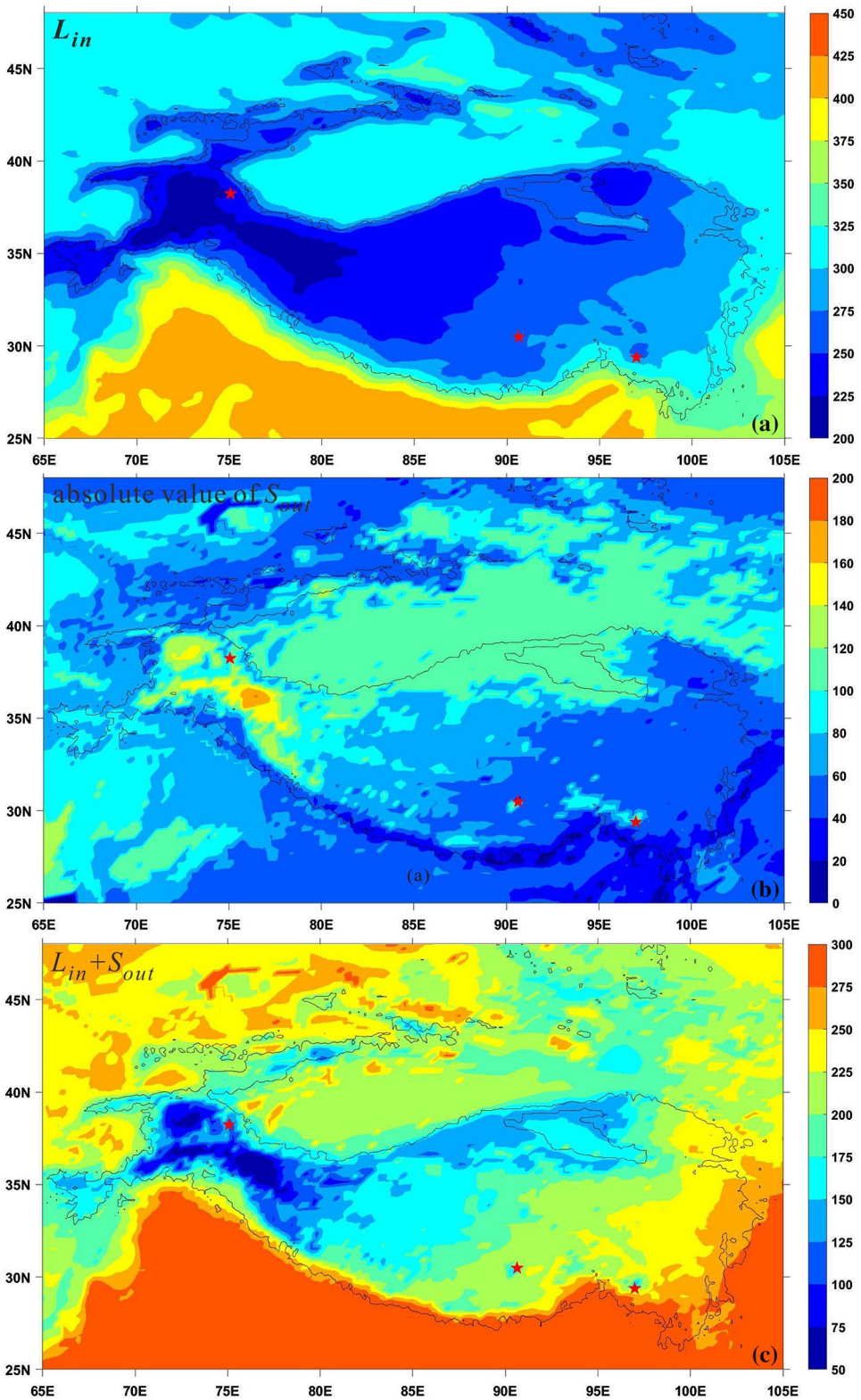


**Fig. 12** Mean incoming longwave radiation (**a**), absolute value of outgoing shortwave radiation (**b**) and sum of incoming longwave radiation and outgoing shortwave radiation (**c**) for July to September during 2000 and 2013 (all data are from the HAR30, unit: W/m$^2$)

season. These conditions led to acceleration of the snow melt on the glacier surface, and finally low $\alpha$ (0.56 and 0.56) values appeared on these two glaciers. As part of the feedback associated with surface snow albedo (Oerlemans et al. 2009), more solar radiation is absorbed for snowmelt due to a low value of $\alpha$, which in turn accelerates the disappearance of the snowpack. In contrast, higher values of $\alpha$ (0.73) occurred on MZ15 glacier, because the low $T_a$ values

on MZ15 glacier resulted in almost all of the precipitation falling as snow and lower $L_{in}$ and turbulent heat fluxes, which further slows down the melting of surface snow. On the whole, the spatial distribution of $L_{in}$+$S_{out}$ is consistent with that of glacier mass balance changes on the TP. The regional differences in $L_{in}$ and $S_{out}$ are related to local climate conditions, especially for $T_a$.

### 5.3 Comparison of glacier energy balance from different studies

Although some in situ measurements of point surface energy-balance are available (e.g. Yang et al. 2011; Zhu et al. 2015), analyses of glacier-wide energy balances are very few. To compare the surface energy fluxes with values from other glaciers, we collected published energy flux data obtained from different glaciers on the TP (Table 7). The $H_{lat}$ value reported by Huintjes (2014) is significantly larger than that of the other studies due to different empirical methods and data that they used to calculated turbulent heat flux. However, the $S_{net}$, $L_{net}$, $H_{sen}$, $QG$ and $Q_M$ values for ZD glacier reported by Huintjes (2014), Zhang et al. (2016a), Mölg et al. (2012) and this study are similar (Table 7). Moreover, the differences in these energy balance components are smaller than 10 W/m$^2$. Because sufficient observational meteorological data and mass balance data are available on ZD glacier, the modelled results of Huintjes (2014) are close to observations on ZD glacier. But for MZ15 glacier in this study and Muztag Ata No. 16 (MZ16) glacier in Huintjes (2014) (these two glaciers are adjacent to each other), the values of $H_{sen}$, $Q_G$ and $Q_M$ are similar, but the values of $S_{net}$, $L_{net}$ and $H_{lat}$ are remarkably different. And the modelled annual mean mass balance during 2001–2012 obtained from Huintjes (2014) is larger than the values during 1999–2013 from Holzer et al. (2015) and Zhang et al. (2016b), who obtained values from the different periods of DEM. The results obtained for MZ16 glacier by Huintjes (2014) required them to constrain their modelling using some kind of meteorological, glaciological or remote sensing-based field observations. Although the values are different in both studies, they both show the basic characteristics of energy balance in the Muztag Ata region with a small absolute value of $Q_M$ and large absolute value of $H_{lat}$. In addition, according to the data from the five glaciers presented by Huintjes (2014), linear correlation between ($L_{in}$+$S_{out}$) and $Q_M$ ($Q_M$=-0.2078*($L_{in}$+$S_{out}$)-0.5406, R²=0.9211) is good. This result verifies that ($L_{in}$+$S_{out}$) is a good index for $Q_M$ and surface melt.

### 5.4 Factors controlling the sensitivity of glacier mass balance to air temperature change

The annual mean $T_a$ values on the TP increased by 0.04 °C a$^{-1}$ from 1960 to 2013 (Zhang et al. 2015). Data obtained from the CMS near glaciers indicate that the three study regions have all experienced significant warming over the past several decades (Fig. 13). The response of mass balance to warming varies in different climatic regions for the three glaciers on the TP. In terms of $T_a$ change, both PL04 and ZD glaciers in the southern portion of the TP were influenced by the SAM and show higher mass balance sensitivity to $T_a$ change than that of MZ15 glacier, which lies in the northwest portion of the TP and is influenced by the westerlies on the TP. Moreover, even though those glaciers are located in the westerly region, the sensitivity of mass balance to $T_a$ change is still different. The sensitivity of glacier mass balance to $T_a$ change is only between 0.2 and 0.5 m w.e. a$^{-1}$ °C$^{-1}$ in the Tianshan mountains (Liu et al. 1998; Rasmussen 2013). In addition, this quantity is only 0.38–0.56 w.e. a$^{-1}$ °C$^{-1}$ on Qiyi glacier (Jiang et al. 2010; Wang et al. 2012). Above all, the sensitivity of glacier mass balance to $T_a$ change differs in different regions. Three factors could help to explain the sensitivity differences among TP glaciers to $T_a$ change.

First, the most important factor in determining the different sensitivities of glacier mass balance to $T_a$ change is the difference in the ratio of snowfall to precipitation, which is related to difference in snowfall change during the ablation season in the different regions. Oerlemans (2001) found that the ratio of snowfall to precipitation was related to the higher sensitivity of mass balance in wetter environments. Anderson et al. (2010) found that on a marine glacier in New Zealand, 60% of mass balance sensitivity to $T_a$ change resulted from the ratio of snowfall to precipitation. In general, changing the ratio of snowfall to precipitation is not only related to accumulation variations, but it also strongly

**Table 7** Comparison of annual mean energy fluxes (W/m$^2$) of glaciers on the Tibetan Plateau at the glacier-wide scale

| | Period | $S_{net}$ | $L_{net}$ | $H_{sen}$ | $H_{lat}$ | $QG$ | $Q_M$ |
|---|---|---|---|---|---|---|---|
| ZD glacier Zhang et al. (2016a) | 2011–2014 | 66.9 | −46.9 | 18.6 | −9.1 | 1.1 | −30.6 |
| ZD glacier Huintjes (2014) | 2002–2011 | 73.6 | −51.4 | 24.6 | −35 | −3.6 | −13.2 |
| ZD glacier (this study) | 2008–2013 | 69 | −49 | 14 | −13 | −1 | −20 |
| ZD glacier Mölg et al. (2012) | 2009–2011 | 72.7 | −67.3 | 17.9 | −10.9 | 1.1 | −13.7 |
| MZ15 glacier Huintjes (2014) | 2001–2011 | 29.8 | −42 | 13.3 | −0.8 | −1.9 | −0.4 |
| MZ16 glacier (this study) | 2008–2013 | 69 | −61 | 18 | −24 | 0 | −2 |

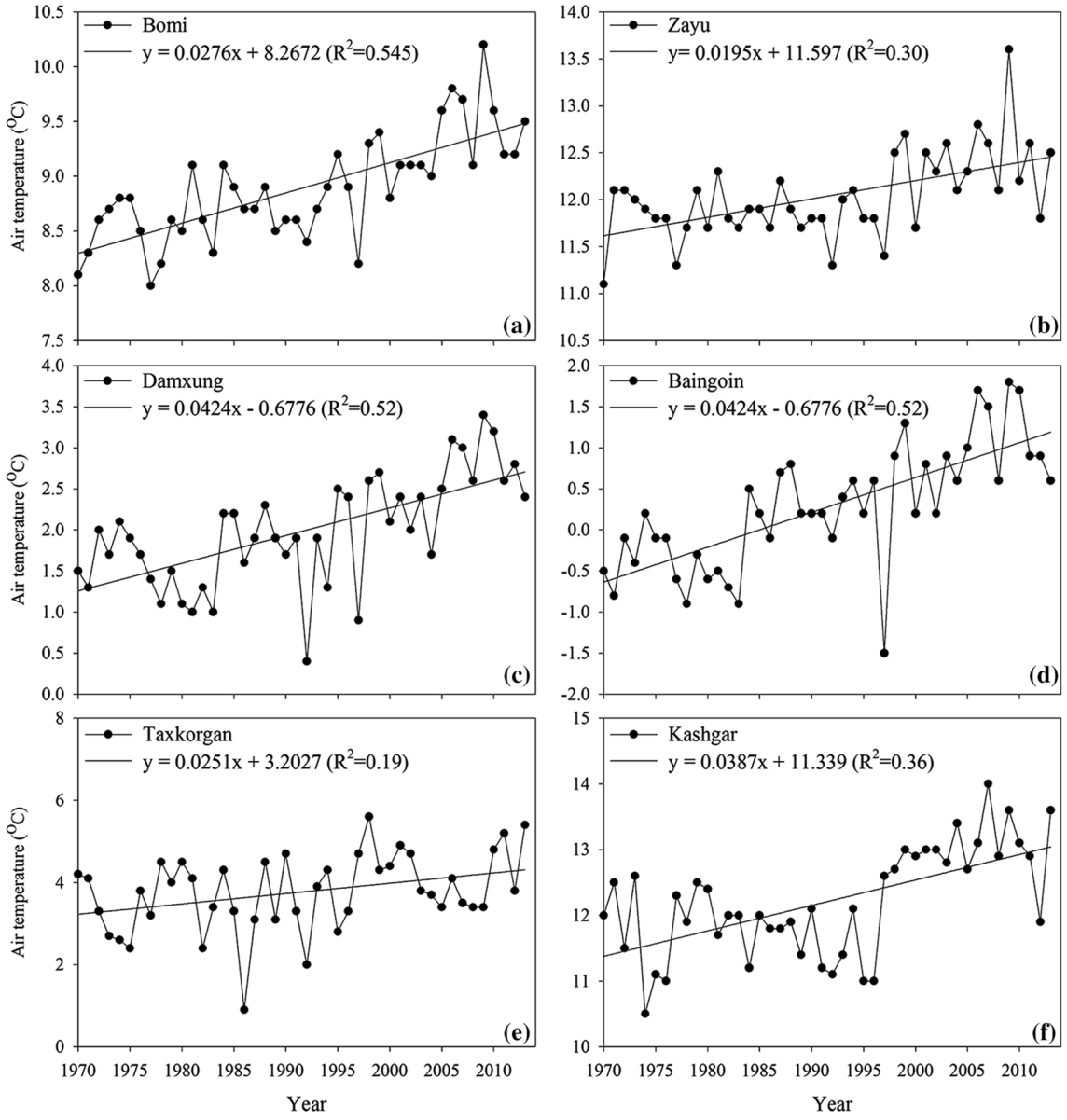


**Fig. 13** Annual mean air temperature at Bomi (**a**), Zayu (**b**), Damxung (**c**), Baingoin (**d**), Taxkorgan (**e**) and Kashgar (**f**) from 1970 to 2013

influences changes in $\alpha$ by driving changes in snowfall. In addition, $\alpha$ was the most important factor in driving glacier mass balance changes (Favier et al. 2004; Huintjes 2014; Yang et al. 2011). These processes significantly influence the sensitivity of glacier mass balance to $T_a$ change through the ratio of snowfall to precipitation changes. During the ablation season, 50% and 83% of precipitation fall as snow on PL04 and ZD glaciers. The ratio of snowfall to precipitation is highly dependent on $T_a$ change for PL04 and ZD glaciers. As $T_a$ is slightly higher than $T_{snow}$ (Tables 3, 4), small changes in $T_a$ would result in a large change in the proportion of precipitation into snowfall. A 1 °C increase (or decrease) in $T_a$ resulted in a decrease (or increase) of 22% (or 23%) and 15% (or 16%) in snowfall on PL04 and ZD glaciers. However, for MZ15 glacier, the ratio of snowfall to precipitation and snowfall was almost unaffected by increases in $T_a$; that is, it is less sensitive to warming. In other words, snowfall is influenced by $P$ and not by $T_a$ on MZ15 glacier. This result is in agreement with that of Huintjes (2014). Because $T_a$ is significantly lower than $T_{snow}$ (Tables 3, 4), almost all precipitation falls as snow on MZ15 glacier. A 1 °C increase in $T_a$ results in a decrease of only 1% in the ratio of snowfall to precipitation and a 2% decrease in snowfall. Compared to MZ15 glacier, a lower ratio of snowfall to precipitation during the ablation season leads to a greater decrease in snowfall on the other two

glaciers and a change in the annual mean $\alpha$ from 0.64 to 0.59 on PL04 glacier and from 0.66 to 0.62 on ZD glacier when $T_a$ increases by 1 °C. Further, higher mass losses, and finally an increased sensitivity of mass balance to $T_a$ change occurred on PL04 and ZD glaciers.

Second, differences in melt energy ($L_{in}$+$S_{out}$) during the ablation season is another important factor that drive the different sensitivities of Tibetan glaciers to $T_a$ change. Melt energy is substantially higher on PL04 and ZD glaciers than on MZ15 glacier. This mean that faster melting of snow cover and snowfall occur on PL04 and ZD glaciers, which causes lower values of $\alpha$ and more snow/ice melt, and further leads to larger mass losses on these two glaciers. In addition, strong melting occurs from June to September on PL04 and ZD glaciers; however, strong melting occurs only from July to August on MZ15 glacier. The longer ablation season melts the snow cover earlier and the bare ice surface is maintained longer on PL04 and ZD glaciers. Lastly, $L_{in}$ and turbulent heat fluxes increase more on PL04 and ZD glaciers than MZ15 glacier when $T_a$ increases by 1 °C. In addition, a great increase of $L_{in}$ and turbulent heat fluxes provides more melt energy on PL04 and ZD glaciers. These processes, enhanced by the albedo feedback, contribute to the larger mass losses and higher sensitivities to $T_a$ change noted for PL04 and ZD glaciers.

Third, differences in the seasonal distribution of precipitation also play a role in producing the different sensitivities of mass balance of Tibetan glaciers to $T_a$ change. Although the ratio of snowfall to precipitation is lower, and the amount of melt energy is slightly higher on PL04 glacier than on ZD glacier, the sensitivity of mass balance to $T_a$ change on both glaciers is similar. The large amounts of $P$ that occur in spring on PL04 glacier could protect this glacier from changes in $T_a$ (Yang et al. 2013) because the amount of $P$ in spring is almost unaffected by $T_a$ change. Thus, $P$ in spring reduces mass balance sensitivity to $T_a$ change on PL04 glacier. This is why both glaciers have almost the same sensitivity to $T_a$ change when the ratio of snowfall to precipitation and melt energy are significantly different from each other. Fujita and Ageta (2000) also indicated that summer-accumulation-type glaciers displayed a higher mass balance sensitivity to $T_a$ change than winter accumulation glaciers.

These analyses imply that the variations in the above three factors are important in determining glacier mass balance changes under global warming. Indeed, the above three factors, especially the ratio of snowfall to precipitation and the amount of melt energy during the ablation season, could help explain the spatial differences in glacier mass balance change in different regions under global warming on and around the TP. Figure 14 shows the mean ratio of snowfall to precipitation for the ablation season and throughout the year on and around the TP. Snowfall and precipitation data used here were extracted from the HAR30 dataset. Figure 14a shows the low ratio of snowfall to precipitation during the ablation season for the Karakoram mountains. There, most precipitation falls in winter and spring, and almost no precipitation falls in summer (Maussion et al. 2013). Thus, snowfall amount is not influenced by an increase in $T_a$, or it is less sensitive to warming (Kapnick et al. 2014). Therefore, the Karakoram mountains are identified as a region with a high ratio of snowfall to precipitation during the ablation season; this region appears to be less influenced by increasing $T_a$ on snowfall. Figure 14b shows that the annual mean ratio of snowfall to precipitation is higher in some regions, such as the western Himalaya mountains, some regions of the southeast TP and some regions of the Tianshan mountains. This is due to tje high ratio of snowfall to precipitation that occurs in these regions during the cold season, especially spring. However, more precipitation occurred during the ablation season than that during the cold season in these regions (Maussion et al. 2013). Therefore, these regions are identified as the regions with a low ratio of snowfall to precipitation during the ablation season due to significant decreases in snowfall in these regions caused by warming (Fig. 14a).

Figures 12c and 14a show that the regions with low (or high) ratios of snowfall to precipitation are characterized by high (or low) amounts of melt energy ($L_{in}$+$S_{out}$). The ratio of snowfall to precipitation is closely related to precipitation and air temperature. These two climate factors are also related to $L_{in}$ and $S_{out}$. It is not possible to separate the influences of these two factors on mass balance sensitivity. From an overall perspective, when compared to the northern TP, especially the northwestern TP, lower ratios of snowfall to precipitation and higher melt energy ($L_{in}$+$S_{out}$) during the ablation season occurred on the southern TP, which is influenced by the SAM. This observation indicates that sensitivity and glacier mass loss are higher in the southern TP under global warming (Kääb et al. 2015; Neckel et al. 2014; Yao et al. 2012).

In addition, the ratio of snowfall to precipitation and melt energy during the ablation season shows spatial differences for glaciers in different regions, and these differences are linked to spatial differences in Tibetan glacier mass balance changes. First, in the eastern Pamir, the Karakoram mountains and the western Kunlun mountains the ratio of snowfall to precipitation is high, and the amount of melt energy is low (Figs. 14a, 12c). Glacier mass losses are small in these regions; some glaciers in these areas have gained mass under global warming (Kääb et al. 2015; Kapnick et al. 2014; Neckel et al. 2014; Yao et al. 2012). In the central Tianshan mountains, the eastern Kunlun mountains and the Altun mountains the ratio of snowfall to precipitation and melt energy is second to largest. In these regions, glacier mass losses are moderate. Farinotti et al. (2015)

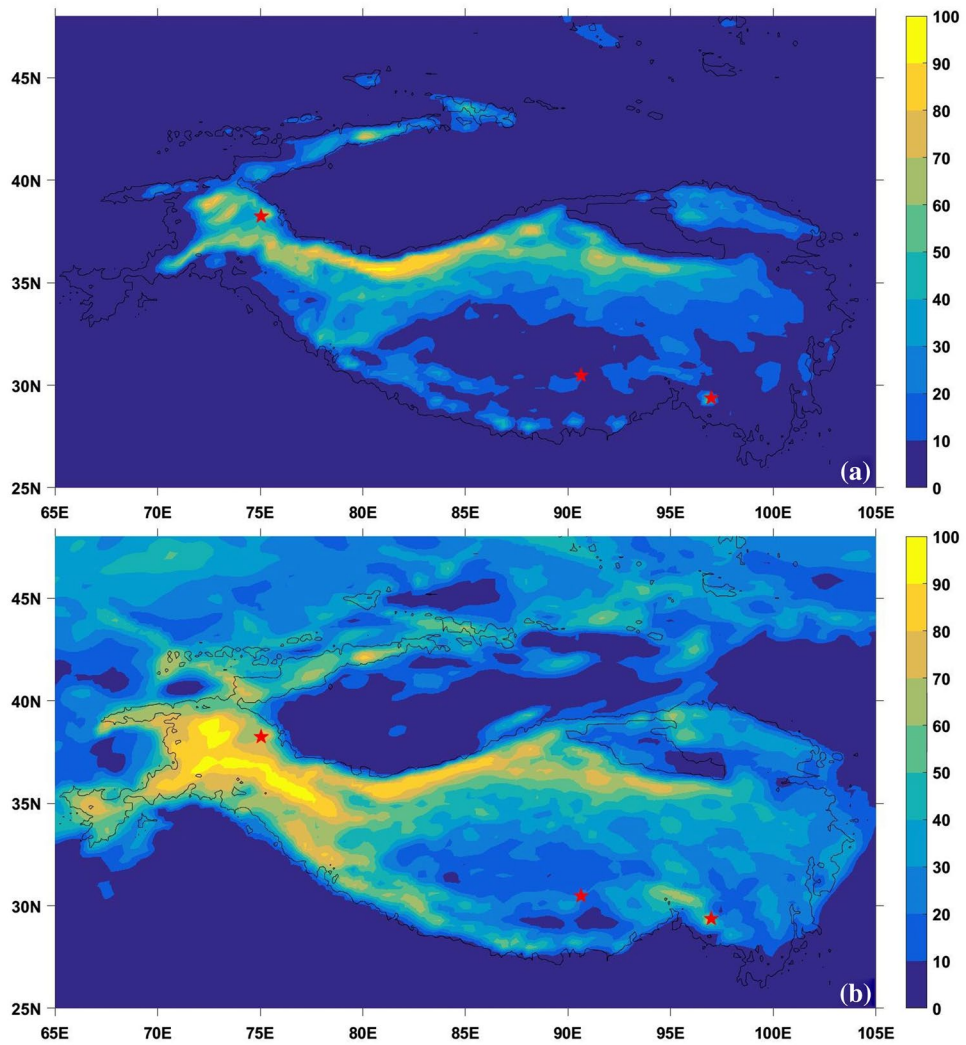


**Fig. 14** Mean ratio of snowfall to precipitation during the ablation season (**a**) and year-round (**b**) from 2001 to 2013 on the TP. Snowfall and precipitation are from the HAR30. In addition, the red stars indicate locations of the three glaciers

noted small rates of glacier mass losses occurred in the central Tianshan mountains. Finally, the ratio of snowfall to precipitation is less than 50%, and $L_{in}$+$S_{out}$ is larger than 200 W/m$^2$, in other regions, such as most parts of the Tianshan mountains, the Qilian mountains (especially the eastern Qilian mountains), the southeast TP (which contains the Hengduan mountains), Himalaya mountains (especially eastern Himalayas), the Nyainqêntanglha mountains and the Tanggula mountains, where glacier mass loss has increased with global warming. In particular, the southeastern TP, the Himalaya mountains, the Nyainqêntanglha mountains and the Tanggula mountains, which are influenced by the SAM and have the lowest ratio of snowfall to precipitation and the highest melt energy during the ablation season, are associated with the most intensive mass losses. The large mass losses of glaciers in these regions were noted by Yao et al. (2012), Neckel et al. (2013) and Kääb et al. (2015).

Above all, glacier mass balance sensitivity to $T_a$ change differs on and around the regions of the TP. These differing sensitivities are mainly caused by differences in the ratio of snowfall to precipitation during the ablation season, the amount of melt energy during the ablation season and precipitation seasonality among the different regions. And these three factors are related to local climatic conditions, especially $T_a$.

Our findings provide insight into the major drivers of spatial heterogeneity of mass balance for Tibetan glaciers under global warming. Glaciers in most regions of the TP, especially the SAM region, show high sensitivity to $T_a$ change, which means that large ice losses occur even under moderate climate warming. Within these regions, $T_a$ is more important than $P$ in determining glacier mass change. Glaciers in the Muztag Ata region show a lower sensitivity to $T_a$ change, and its sensitivity to $P$ change is slightly higher than that of $T_a$ change. Thus, glaciers in this dry and cold region remain stable, or even increase in mass when regional climate change leads to increased precipitation and overall slightly warmer conditions which have been found on and around the TP (Kapnick et al. 2014; Zhang et al.

2017). In addition, these wet and warm climatic conditions may have occurred in the Karakoram mountains and the western Kunlun mountains, given the small change of glacier area and volume found in these regions (Gardelle et al. 2013; Kääb et al. 2015; Kapnick et al. 2014; Ke et al. 2015; Neckel et al. 2014).

## 6 Conclusion

Based on a physical EMB model, the glacio-meteorological measurements and mass balance stake records from PL04, ZD and MZ15 glaciers, meteorology, mass and energy balance characteristics of three selected glaciers were comparatively analyzed from October 1st, 2008 to September 21st, 2013. This analysis show that surface melt is the largest source of differences in mass balance between PL04 and ZD glaciers and MZ15 glacier. $S_{out}$ (or $\alpha$) and $L_{in}$ are the most important factors controlling the differences in melt energy. The differences in these factors are due to climatic conditions that occur in the different regions, such as $T_a$, humidity, $P$ and cloudiness. Moreover, the spatial distribution of $L_{in}$+$S_{out}$ is consistent with glacier mass balance changes on the TP. In addition, there is a small difference in mass balance between PL04 and ZD glaciers that results from differences in snowfall, especially snowfall during the cold season.

According to the model, climate sensitivity tests were performed. These tests show that the sensitivity of mass balance to $T_a$ change is significantly larger than that to $P$ change on PL04 and ZD glaciers. However, on MZ15 glacier the sensitivity of mass balance to $T_a$ change is slightly lower than that to $P$ change. In addition, the sensitivity of mass balance to $T_a$ change on MZ15 glacier is significantly lower than that on PL04 and ZD glaciers. These differences in glacier mass balance sensitivity to $T_a$ change are caused by differences in the ratio of snowfall to precipitation during the ablation season, melt energy (or $L_{in}$+$S_{out}$) during the ablation season and precipitation seasonality in the different regions of the TP. The differences in the ratio of snowfall to precipitation and melt energy result from the different climate conditions that occur in the different regions on the TP, especially $T_a$. On PL04 and ZD glaciers $T_a$ is slightly higher than $T_{snow}$, but on MZ15 glacier $T_a$ is lower than $T_{snow}$. Thus, a low ratio of snowfall to precipitation and high melt energy are found for PL04 and ZD glaciers. A slight increase in $T_a$ results in a substantial reduction of $\alpha$ through significantly decreasing the amount of snowfall during the ablation season; further, it greatly increases melt energy, and these processes cause high glacier mass losses on PL04 and ZD glaciers. However, glaciers in the Muztag Ata region show a high ratio of snowfall to precipitation and low melt energy during the ablation season. Increasing $T_a$ slightly reduces the amount of snowfall and produces a small decrease of $\alpha$ and a small increase in melt during the ablation season. Thus, small mass losses occur on MZ15 glacier under the concurrent warming.

These three factors can explain the different patterns of Tibetan glacier mass balance changes under global warming, especially the ratio of snowfall to precipitation and melt energy during the ablation season. It is not possible to separate the effects of these two factors on mass balance sensitivity because regions with low (or high) ratios of snowfall to precipitation during the ablation season are characterized by high (or low) melt energy ($L_{in}$+$S_{out}$). Glaciers in regions with a low ratio of snowfall to precipitation and high melt energy are more sensitive to $T_a$ change. Examples include most regions of the Tianshan mountains and the Qilian mountains and especially the SAM regions. Glaciers in these regions occur large mass losses under the wet and warm climatic scenario. In contrast, glaciers in regions with high ratio of snowfall to precipitation and low melt energy are relatively insensitive to $T_a$ change and experience smaller mass losses, such as the Karakoram mountains, the eastern Pamir and the western Kunlun mountains. Glaciers in these dry and cold regions remain stable, or even increase in mass when regional climate change leads to increased precipitation and overall slightly warmer conditions. The above statements can be used to provide insight into the major drivers of spatial heterogeneity of mass balance changes for Tibetan glaciers under significant recent warming. Finally, it is worthwhile to note that this comparison involves only three glaciers over a period of five years, and further comparisons involving more glaciers on the TP over a longer time scale are needed.

**Acknowledgements** We acknowledge the staff at the Muztagh Ata Station for Westerly Environment Observation and Research and the Nam Co Monitoring and Research Station for Multisphere Interactions, Institute of Tibetan Research, Chinese Academy of Sciences, for help in the field. We thank the Third Pole Environment Database, Institute of Tibetan Research, Chinese Academy of Sciences and the National Climate Center, China Meteorological Administration, for providing the climate data used herein. We thank two anonymous reviewers for valuable insights that greatly strengthened the manuscript. We thank Dieter Scherer and Julia Curio (Technical University of Berlin) and Fabien Maussion (University of Innsbruck) for providing the HAR data, and Kun Yang (Institute of Tibetan Research, Chinese Academy of Sciences) for providing the CMFD data. The SRTM data and the Landsat data were provided by the US Geological Survey. This study was jointly funded by the National Natural Science Foundation of China (Grant Nos. 41190081, 91547104, 41601081, 91647205, 41371085, and 41125003) and the China Postdoctoral Science Foundation (Grant No. 2017M611014).

## References

Anderson B, Mackintosh A, Stumm D, George L, Kerr T, Winter-Billington A, Fitzsimons S (2010) Climate sensitivity

of a high-precipitation glacier in New Zealand. J Glaciol 56(195):114–128. doi:10.3189/002214310791190929
Arnold N, Willis I, Sharp M, Richards K, Lawson W (1996) A distributed surface energy-balance model for a small valley glacier. I. Development and testing for Haut Glacier d'Arolla, Valais, Switzerland. J Glaciol 42(140):77–89
Ayala A, Pellicciotti F, Shea JM (2015) Modeling 2 m air temperatures over mountain glaciers: exploring the influence of katabatic cooling and external warming. J Geophys Res 120(8):3139–3157. doi:10.1002/2015JD023137
Barral H, Genthon C, Trouvilliez A, Brun C, Amory C (2014) Blowing snow in coastal Adélie Land, Antarctica: three atmospheric-moisture issues. Cryosphere 8:1905–1919 doi:10.5194/tc-8-1905-2014
Bintanja R, Reijmer CH (2001) A simple parameterization for snowdrift sublimation over Antarctic snow surfaces. J Geophys Res 106(D23):31739–31748. doi:10.1029/2000JD000107
Bolch T, Yao T, Kang S, Buchroithner MF (2010) A glacier inventory for the western Nyainqentanglha Range and the Nam Co Basin, Tibet, and glacier changes 1976–2009. Cryosphere 4:419–433 doi:10.5194/tc-4-419-2010
Bolch T, Kulkarni A, Kääb A, Huggel C, Paul F, Cogley J, Frey H, Kargel J, Fujita K, Scheel M (2012) The State and Fate of Himalayan Glaciers. Science 336(6079):310–314. doi:10.1126/science.1215828
Brock BW, Arnold NS (2000) A spreadsheet-based (Microsoft Excel) point surface energy balance model for glacier and snow melt studies. Earth Surf Proc Land 25(6):649–658. doi:10.1002/1096-9837(200006)25:6<649::aid-esp97>3.0.co;2-u
Cao B (2013) Glacier variation in the Lenglongling range of eastern Qilian mountains. PhD thesis, University of Lanzhou (in Chinese with English abstract)
Crawford TM, Duchon CD (1999) An improved parameterization for estimating effective atmospheric emissivity for use in Calculating Daytime Downwelling Longwave Radiation. J Appl Meteorol 38(4):474–480
Ding B, Yang K, Qin J, Wang L, Chen Y, He X (2014) The dependence of precipitation types on surface elevation and meteorological conditions and its parameterization. J Hydrol 513:154–163. doi:10.1016/j.jhydrol.2014.03.038
Farinotti D, Longuevergne L, Moholdt G, Duethmann D, Mölg T, Bolch T, Vorogushyn S, Güntner A (2015) Substantial glacier mass loss in the Tien Shan over the past 50 years. Nat Geosci 8:716–722 doi:10.1038/ngeo2513
Favier V, Wagnon P, Ribstein P (2004) Glaciers of the outer and inner tropics: A different behaviour but a common response to climatic forcing. Geophys Res Lett 31:L16403. doi:10.1029/2004GL020654
Fujita K, Ageta Y (2000) Effect of summer accumulation on glacier mass balance on the Tibetan Plateau revealed by mass-balance model. J Glaciol 46(153):244–252. doi:10.3189/172756500781832945
Fujita K, Nuimura T (2011) Spatially heterogeneous wastage of Himalayan glaciers. Proc Natl Acad Sci USA 108(34):14011–14014. doi:10.1073/pnas.1106242108
Fujita K, Sakai A (2014) Modelling runoff from a Himalayan debris-covered glacier. Hydrol Earth Syst Sci 18:2679–2694. doi:10.5194/hess-18-2679-2014
Gardelle J, Berthier E, Arnaud Y, Kääb A (2013) Region-wide glacier mass balances over the Pamir-Karakoram-Himalaya during 1999–2011. Cryosphere 7:1263–1286 doi:10.5194/tc-7-1263-2013
Gardner AS, Moholdt G, Cogley JG, Wouters B, Arendt AA, Wahr J, Berthier E, Hock R, Pfeffer WT, Kaser G, Ligtenberg SR, Bolch T, Sharp MJ, Hagen JO, van den Broeke MR, Paul F (2013) A reconciled estimate of glacier contributions to sea level rise: 2003 to 2009. Science 340(6134):852–857. doi:10.1126/science.1234532
Giesen R, Van den Broeke M, Oerlemans J, Andreassen L (2008) Surface energy balance in the ablation zone of Midtdalsbreen, a glacier in southern Norway: interannual variability and the effect of clouds. J Geophys Res 113:D21208. doi:10.1029/2008JD010390
Greuell W, Böhm R (1998) 2 m temperatures along melting mid-latitude glaciers, and implications for the sensitivity of the mass balance to variations in temperature. J Glaciol 44(146):9–20
Guo W, Liu S, Yao X, Xu J, Shangguan D, Wu L, Zhao J, Liu Q, Zongli Jiang Z, Wei J, Bao W, Yu P, Ding L, Li G, Li P, Ge C, Wang Y (2014) The second glacier inventory dataset of China (version 1.0). Cold and Arid Regions Science Data Center: Lanzhou, China doi:10.3972/glacier.001.2013.db
Guo W, Liu S, Xu J, Wu L, Shangguan D, Yao X, Wei J, Bao W, Yu P, Liu Q, Jiang Z (2015) The second Chinese glacier inventory: data, methods and results. J Glaciol 61(226):357–372. doi:10.3189/2015JoG14J209
Guo X, Wang L, Tian L (2016) Spatio-temporal variability of vertical gradients of major meteorological observations around the Tibetan Plateau International. J Climatol 36(4):1901–1916. doi:10.1002/joc.4468
He J, Yang K (2011) China meteorological forcing dataset cold and arid regions science data center at Lanzhou. doi:10.3972/westdc.002.2014.db
Hewitt K (2005) The Karakoram Anomaly? Glacier Expansion and the 'Elevation Effect,' Karakoram Himalaya. Mt Res Dev 25(4):332–340 doi:10.1659/0276-4741(2005)025[0332:TKAGEA]2.0.CO;2
Hock R, Holmgren B (2005) A distributed surface energy-balance model for complex topography and its application to Storglaciaren, Sweden. J Glaciol 51(172):25–36. doi:10.3189/172756505781829566
Holzer N, Vijay S, Yao T, Xu B, Buchroithner M, Bolch T (2015) Four decades of glacier variations at Muztagh Ata (eastern Pamir): a multi-sensor study including Hexagon KH-9 and Pléiades data. Cryosphere 9:2071–2088 doi:10.5194/tc-9-2071-2015
Huintjes E (2014) Energy and mass balance modelling for glaciers on the Tibetan Plateau: extension, validation and application of a coupled snow and energy balance model. PhD thesis, RWTH Aachen University, P 222, http://publications.rwth-aachen.de/record/459462
Huintjes E, Sauter T, Schröter B, Maussion F, Yang W, Kropáček J, Buchroithner M, Scherer D, Kang S, Schneider C (2015) Evaluation of a Coupled Snow and Energy Balance Model for Zhadang Glacier, Tibetan Plateau, Using Glaciological Measurements and Time-Lapse Photography. Arct Antarct Alp Res 47(3):573–590. doi:10.1657/AAAR0014-073
Immerzeel WW, van Beek LPH, Bierkens MFP (2010) Climate Change Will Affect the Asian Water Towers. Science 328(5984):1382–1385. doi:10.1126/science.1183188
Jiang X, Wang N, He J, Wu X, Song G (2010) A distributed surface energy and mass balance model and its application to a mountain glacier in China. Chin Sci Bull 55(20):2079–2087 doi:10.1007/s11434-010-3068-9
Kääb A, Treichler D, Nuth C, Berthier E (2015) Brief Communication: Contending estimates of 2003–2008 glacier mass balance over the Pamir–Karakoram–Himalaya. Cryosphere 9:557–564 doi:10.5194/tc-9-557-2015
Kapnick SB, Delworth TL, Ashfaq M, Malyshev S, Milly PCD (2014) Snowfall less sensitive to warming in Karakoram than in Himalayas due to a unique seasonal cycle. Nat Geosci 7:834–840 doi:10.1038/ngeo2269
Ke L, Ding X, Song C (2015) Heterogeneous changes of glaciers over the western Kunlun Mountains based on ICESat and Landsat-8 derived glacier inventory. Remote Sens Environ 168:13–23

Li B, Yu Z, Liang Z, Acharya K (2014) Hydrologic response of a high altitude glacierized basin in the central Tibetan Plateau. Global Planet Change 118(4):69–84. doi:10.1016/j.gloplacha.2014.04.006

Li B, Acharya K, Yu Z, Liang Z, Su F (2015) The Mass and Energy Exchange of a Tibetan Glacier: Distributed Modeling and Climate Sensitivity. J Am Water Resour As 51(4):1088–1100. doi:10.1111/jawr.12286

Li S, Yao T, Yang W, Yu W, Zhu M (2016) Melt season hydrological characteristics of the Parlung No. 4 Glacier, in Gangrigabu Mountains, south-east Tibetan Plateau. Hydrol Process 30(8):1171–1191. doi:10.1002/hyp.10696

Liu X, Chen B (2000) Climatic warming in the Tibetan Plateau during recent decades. Int J Climatol 20(14):1729–1742. doi:10.1002/1097-0088(20001130)20:14<1729::AID-JOC556>3.0.CO;2-Y

Liu Q, Liu S (2015) Response of glacier mass balance to climate change in the Tianshan Mountains during the second half of the twentieth century. Clim Dyn 46(1–2):303–316 doi:10.1007/s00382-015-2585-2

Liu S, Ding Y, Wang N, Xie Z (1998) Mass balance sensitivity to climate change of the Glacier No. 1 at the Urumqi River Head, Tianshan mountains. J Glaciol Geocryol 20(1):9–13 (**Chinese with English abstract**)

Ma Y, Zhang Y, Yang D, Farhan SB (2015) Precipitation bias variability versus various gauges under different climatic conditions over the Third Pole Environment (TPE) region. Int J Climatol 35(7):1201–1211. doi:10.1002/joc.4045

Maussion F, Scherer D, Mölg T, Collier E, Curio J, Finkelnburg R (2013) Precipitation Seasonality and Variability over the Tibetan Plateau as Resolved by the High Asia Reanalysis. J Clim 27(5):1910–1927. doi:10.1175/JCLI-D-13-00282.1

Mölg T, Hardy DR (2004) Ablation and associated energy balance of a horizontal glacier surface on Kilimanjaro. J Geophys Res 109:D16104. doi:10.1029/2003JD004338

Mölg T, Cullen NJ, Hardy DR, Kaser G, Klok L (2008) Mass balance of a slope glacier on Kilimanjaro and its sensitivity to climate. Int J Climatol 28(7):881–892. doi:10.1002/joc.1589

Mölg T, Maussion F, Yang W, Scherer D (2012) The footprint of Asian monsoon dynamics in the mass and energy balance of a Tibetan glacier. Cryosphere 6:1445–1461 doi:10.5194/tc-6-1445-2012

Mölg T, Maussion F, Scherer D (2014) Mid-latitude westerlies as a driver of glacier variability in monsoonal High Asia. Nat Clim Change 4(1):68–73 doi:10.1038/Nclimate2055

Neckel N, Kropáček J, Bolch T, Hochschild V (2014) Glacier mass changes on the Tibetan Plateau 2003–2009 derived from ICESat laser altimetry measurements. Environ res lett 9(1):014009. doi:10.1088/1748-9326/9/1/014009

Nicholson LI, Prinz R, Mölg T, Kaser G (2013) Micrometeorological conditions and surface mass and energy fluxes on Lewis Glacier, Mt Kenya, in relation to other tropical glaciers. Cryosphere 7:1205–1225 doi:10.5194/tc-7-1205-2013

Oerlemans J (2001) Glaciers and climate change. AA Balkema Publishers, Rotterdam

Oerlemans J, Anderson B, Hubbard A, Huybrechts P, Johannesson T, Knap WH, Schmeits M, Stroeven AP, van de Wal RSW, Wallinga J, Zuo Z (1998) Modelling the response of glaciers to climate warming. Clim Dyn 14:267–274 doi:10.1007/s003820050222

Oerlemans J, Giesen RH, Van Den Broeke MR (2009) Retreating alpine glaciers: increased melt rates due to accumulation of dust (Vadret da Morteratsch, Switzerland). J Glaciol 55(192):729–736. doi:10.3189/002214309789470969

Paterson W (1994) The physics of glaciers, 3rd edn. Oxford Press, Butterworth-Heinemann

Pfeffer WT, Arendt AA, Bliss A, Bolch T, Cogley, JG, Gardner AS, Hagen JO, Hock R, Kaser G, Kienholz C, Miles ES, Moholdt G, Mölg N, Paul F, Radić V, Rastner P, Raup BH, Rich J, Sharp MJ, The Randolph Consortium (2014) The Randolph Glacier Inventory: a globally complete inventory of glaciers. J Glaciol 60(221):537–552 doi:10.3189/2014JoG13J176

Pu J, Yao T, Yang M, Tian L, Wang N, Ageta Y, Fujita K (2008) Rapid decrease of mass balance observed in the Xiao (Lesser) Dongkemadi Glacier, in the central Tibetan Plateau. Hydrol Process 22(16):2953–2958. doi:10.1002/hyp.6865

Radić V, Menounos B, Shea J, Fitzpatrick N, Tessema MA, Déry SJ (2017) Evaluation of different methods to model near-surface turbulent fluxes for an alpine glacier in the Cariboo Mountains, BC, Canada. The Cryosphere Discuss https://doi.org/10.5194/tc-2017-80, in review, 2017

Rasmussen LA (2013) Meteorological controls on glacier mass balance in High Asia. Ann Glaciol 54(63):352–359. doi:10.3189/2013AoG63A353

Reijmer CH, Hock R (2008) Internal accumulation on Storglaciaren, Sweden, in a multi-layer snow model coupled to a distributed energy- and mass-balance model. J Glaciol 54(184):61–72. doi:10.3189/002214308784409161

Rupper S, Roe G, Gillespie A (2009) Spatial patterns of Holocene glacier advance and retreat in Central Asia. Quaternary Res 72(3):337–346

Salerno F, Guyennon N, Thakuri S, Viviano G, Romano E, Vuillermoz E, Cristofanelli P, Stocchi P, Agrillo G, Ma Y, Tartari G (2015) Weak precipitation, warm winters and springs impact glaciers of south slopes of Mt. Everest (central Himalaya) in the last two decades (1994–2013). Cryosphere 9:1229–1247 doi:10.5194/tcd-8-5911-2014

Shi Y, Liu C, Wang Z (2008) Concise Glacier Inventory of China Shanghai. Shanghai Popular Science Press, Shanghai

Sicart JE, Hock R, Ribstein P, Litt M, Ramirez E (2011) Analysis of seasonal variations in mass balance and meltwater discharge of the tropical Zongo Glacier by application of a distributed energy balance model. J Geophys Res 116:D13105. doi:10.1029/2010JD015105

Sun W, Qin X, Ren J, Yang X, Zhang T, Liu Y, Cui X, Du W (2012) The Surface Energy Budget in the Accumulation Zone of the Laohugou Glacier No. 12 in the Western Qilian Mountains, China, in Summer 2009. Arct Antarct Alp Res 44(3):296–305. doi:10.1657/1938-4246-44.3.296

Sun W, Qin X, Du W, Liu W, Liu Y, Zhang T, Xu Y, Zhao Q, Wu J, Ren J (2014) Ablation modeling and surface energy budget in the ablation zone of Laohugou glacier No. 12, western Qilian mountains, China. Ann Glaciol 55(66):111–120. doi:10.3189/2014AoG66A902

Tian H, Yang T, Liu Q (2014) Climate change and glacier area shrinkage in the Qilian mountains, China, from 1956 to 2010. Anna Glaciol 55(66):187–197

Wagnon P, Ribstein P, Francou B, Pouyaud B (1999) Annual cycle of energy balance of Zongo Glacier, Cordillera Real, Bolivia. J Geophys Res 104(D4):3907–3923. doi:10.1029/1998jd200011

Wagnon P, Vincent, C., Arnaud Y, Berthier E, Vuillermoz E, Gruber S, Ménégoz M, Gilbert A, Dumont M, Shea MJ, Stumm D, Pokhrel BK (2013) Seasonal and annual mass balances of Mera and Pokalde glaciers (Nepal Himalaya) since 2007. Cryosphere 7:1769–1786 doi:10.5194/tc-7-1769-2013

Wang N, He J, Pu J, Jiang X, Jing Z (2010) Variations in equilibrium line altitude of the Qiyi Glacier, Qilian Mountains, over the past 50 years. Chin Sci Bull 55(33):3810–3817 doi:10.1007/s11434-010-4167-3

Wang W, Yao T, Yang X (2011) Variations of glacial lakes and glaciers in the Boshula mountain range, southeast Tibet, from the 1970s to 2009. Ann Glaciol 52:9–17

Wang S, Pu J, Wang N (2012) Study on mass balance and sensitivity to climate change in summer on the Qiyi Glacier, Qilian Mountains. Sci Cold Arid Regions 4:281–287 doi:10.3724/SP.J.1226.2012.00281

Wang S, Yao T, Tian L, Pu J (2017) Glacier mass variation and its effect on surface runoff in the Beida River catchment during 1957–2013. J Glaciol 63(239):523–534 doi:10.1017/jog.2017.13

WGMS (2015) Global glacier change bulletin No. 1 (2012–2013). In: Zemp M, Gärtner-Roer I, Nussbaumer SU, Hüsler F, Machguth H, Mölg N, Paul F, and Hoelzle M. (eds.), ICSU(WDS)/IUGG(IACS)/UNEP/UNESCO/WMO, World Glacier Monitoring Service, Zurich, Switzerland, doi:10.5904/wgms-fog-2015-11

Wu X, He J, Jiang X, Wang N (2016) Analysis of surface energy and mass balance in the accumulation zone of Qiyi Glacier, Tibetan Plateau in an ablation season. Environ. Earth Sci 75:1–13. doi:10.1007/s12665-016-5591-8

Xu B, Cao J, Hansenc J, Yao T, Joswia DR, Wang N, Wu G, Wang M, Zhao H, Yang W, Liu X, He J (2009) Black soot and the survival of Tibetan glaciers. Proc Natl Acad Sci USA 106(52):22114–22118 doi:10.1073/pnas.0910444106

Yang W, Yao T, Xu B, Ma L, Wang Z, Wan M (2010) Characteristics of recent temperate glacier fluctuations in the Parlung Zangbo River basin, southeast Tibetan Plateau. Chin Sci Bull 55(20):2097–2102 doi:10.1007/s11434-010-3214-4

Yang W, Guo X, Yao T, Yang K, Zhao L, Li S, Zhu M (2011) Summertime surface energy budget and ablation modeling in the ablation zone of a maritime Tibetan glacier. J Geophys Res 116:D14116. doi:10.1029/2010JD015183

Yang W, Yao T, Guo X, Zhu M, Li S, Kattel DB (2013) Mass balance of a maritime glacier on the southeast Tibetan Plateau and its climatic sensitivity. J Geophys Res 118(17):9579–9594. doi:10.1002/jgrd.50760

Yang W, Guo X, Yao T, Zhu M, Wang Y (2016) Recent accelerating mass loss of southeast Tibetan glaciers and the relationship with changes in macroscale atmospheric circulations. Clim Dyn 47:805–815 doi:10.1007/s00382-015-2872-y

Yao T, Liu X, Wang N, Shi Y (2000) Amplitude of climatic changes in Qinghai-Tibetan Plateau. Chin Sci Bull 45(13):1236–1243

Yao T, Li Z, Yang W, Guo X, Zhu L, Kang S, Wu Y, Yu W (2010) Glacial distribution and mass balance in the Yarlung Zangbo River and its influence on lakes. Chin Sci Bull 55(20):2072–2078

Yao T, Thompson L, Yang W, Yu W, Gao Y, Guo X, Yang X, Duan K, Zhao H, Xu B (2012) Different glacier status with atmospheric circulations in Tibetan Plateau and surroundings. Nat Clim Change 2:663–667 doi:10.1038/nclimate1580

Yu W, Yao T, Kang S, Pu J, Yang W, Gao T, Zhao H, Zhou H, Li S, Wang W, Ma L (2013) Different region climate regimes and topography affect the changes in area and mass balance of glaciers on the north and south slopes of the same glacierized massif (the West Nyainqentanglha Range, Tibetan Plateau). J Hydrol 495:64–73. doi:10.1016/j.jhydrol.2013.04.034

Zafar M, Ahmed M, Rao M, Buckley B, Khan N, Wahab M, Palmer J (2016) Karakorum temperature out of phase with hemispheric trends for the past five centuries. Clim Dyn 46(5–6):1943–1952 doi:10.1007/s00382-015-2685-z

Zhang Y, Hirabayashi Y, Liu S (2012) Catchment-scale reconstruction of glacier mass balance using observations and global climate data: Case study of the Hailuogou catchment, southeastern Tibetan Plateau. J Hydrol 444:146–160. doi:10.1016/j.jhydrol.2012.04.014

Zhang G, Kang S, Fujita K, Huintjes E, Xu J, Yamazaki T, Haginoya S, Yang W, Scherer D, Schneider C, Yao T (2013) Energy and mass balance of Zhadang glacier surface, central Tibetan Plateau. J Glaciol 59(213):137–148. doi:10.3189/2013AoG64A111

Zhang G, Yao T, Xie H, Wang W, Yang W (2015) An inventory of glacial lakes in the Third Pole region and their changes in response to global warming. Global Planet Change 131:148–157. doi:10.1016/j.gloplacha.2015.05.013

Zhang G, Kang S, Cuo L, Qu B (2016a) Modeling hydrological process in a glacier basin on the central Tibetan Plateau with a distributed hydrology soil vegetation model. J Geophys Res 121(16):9521–9539. doi:10.1002/2016JD025434

Zhang Z, Liu S, Wei J, Xu J, Guo W, Bao W, Jiang Z (2016b) Mass Change of Glaciers in Muztag Ata-Kongur Tagh, Eastern Pamir, China from 1971/76 to 2013/14 as Derived from Remote Sensing Data. PloS one 11(1):e0147327. doi:10.1371/journal.pone.0147327

Zhang G, Yao T, Piao S, Bolch T, Xie H, Chen D, Gao Y, O'Reilly CM, Shum CK, Yang K, Yi S, Lei Y, Wang W, He Y, Shang K, Yang X, Zhang H (2017) Extensive and drastically different alpine lake changes on Asia's high plateaus during the past four decades. Geophys Res Lett 44:252–260. doi:10.1002/2016GL072033

Zhu M, Yao T, Yang W, Maussion F, Huintjes E, Li S (2015) Energy- and mass-balance comparison between Zhadang and Parlung No. 4 glaciers on the Tibetan Plateau. J Glaciol 61(227):595–607. doi:10.3189/2015JoG14J206

Zhu M, Yao T, Yang W, Xu B, Wang X (2017) Evaluation of parameterizations of incoming longwave radiation in the high-mountain region of the Tibetan Plateau. J Appl Meteorol Clim 56(4):833–848. doi:10.1175/jamc-d-16-0189.1